From the University of Lund Departments of Anatomy and Diagnostic Radiology, Lund, Sweden

Roentgen stereophotogrammetry

A method for the study of the kinematics of the skeletal system

Göran Selvik

Reprint from the original 1974 thesis

ACTA ORTHOPAEDICA SCANDINAVICA SUPPLEMENTUM NO. 232, VOL. 60. 1989

MUNKSGAARD · COPENHAGEN

Printed in Sweden, Lund 1974
Reprinted
Ortonova
Wallin & Dalholm
Lund 1989

Contents

Introduction

A great number of distances and angles in the human body have been established and recorded by physical anthropology and clinical medicine. These registrations have in most cases been based upon carefully defined measurement points in the object, which has either been some soft-tissue part or a skeletal formation. In this context, measurements on roentgen films, produced in a standardized way, have been carried out for special purposes. The uncertainty in marking the measurement points, however, together with subjective factors during the measurements themselves, can produce errors which are sometimes not negligible.

More precise methods of measurement are required in a number of situations, when measuring the growth of and changes in form of some part of the human body. When using roentgen techniques in such studies, the measurement points have therefore been indicated by implanted radiopaque markers. Even if the relations between roentgen focus, object and film are standardized, however, it is difficult to avoid errors due to varying projections of the object.

The study of the movements in the joints of the human body, is an example where changes in position of one skeletal part in relation to another such part, have been studied by various methods. As a matter of fact, such biomechanical studies represent important parts of functional anatomy. They are also essential in clinical work. Performing such analyses requires:

1) Well-defined concepts of the two basic forms of motion, rotation and translation, and

2) Accurate methods for measuring the movements of the skeletal segments.

An analysis of the basic forms of motion has been made by Hjortsjö (1964), and it was utilized by himself and his co-workers in the study of different joints. The methods of measurement available, however, have not yet allowed registrations with higher accuracy.

The purpose of the present investigation has been to develop a clinical roentgen stereophotogrammetric method which allows:

1) Determination of actual positions of radiopaque markers in an object with high accuracy, and

2) Determination of movements of skeletal segments in terms of rotations and translations.

Acknowledgement

This investigation was supported by grants from the Swedish Medical Research Council (Grant No. 605), the Medical Faculty of the University of Lund and from the Fund for Computer Calculations, the University of Lund.

1. Review of literature

Roentgen stereophotogrammetry

The first trials to determine positions in space from roentgenograms were made a few years after the discovery of roentgen rays. Davidson, a radiologist in London, constructed an apparatus, first described in 1898, for the localization of foreign bodies by means of roentgen rays. His method is as follows: The roentgen tube can be moved on a horizontal bar having a scale. Two fine metal wires are stretched across the examination table below the tube at right angles, and the film or plate to be used is slipped beneath the cross-wires. Two exposures are then made, with the roentgen tube in two different positions on the horizontal bar, on the same roentgen plate and without allowing the patient to move. After being developed, the roentgen negative is taken to another apparatus, called the "localizer". Here it is mounted on a horizontal glass plate, on which two lines have been cut at right angles to each other, corresponding to the metal wires on the examination table. In the localizer there is a horizontal bar, on which two threads of silk are fastened in positions corresponding to the positions of the foci during the two exposures. The threads from the focal positions are stretched to the respective images of the radiopaque object to be studied. The point in space where the threads cross determines the actual positions in space of the object points, as geometric figures in the roentgen apparatus and the localizer are congruent (Figure 1-1).

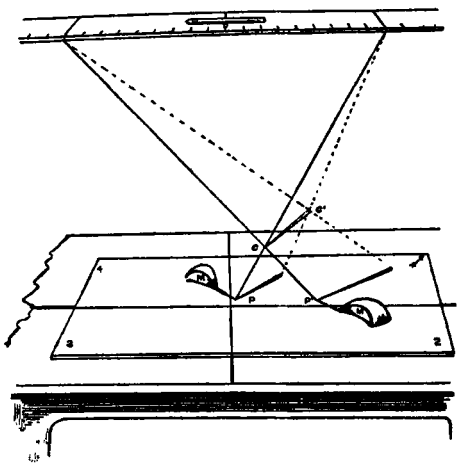

Figure 1-1. Davidson's apparatus ("localizer") with two object points C and C' (needle points) and the two corresponding pairs of crossed threads.

In 1936, Signora Piazzolla-Beloch (professor of mathematics in Ferrara) published an exact counterpart to Davidson's method, but for convergent photography, where the two roentgen films are at right angles to each other.

Piazzolla-Beloch constructed two apparatuses, one for the roentgen exposure, where exposures can be made simultaneously with two tubes, the central rays of which are at right angles to each other. Corresponding to the localizer, she had a second apparatus for the "automatic restitution" of the roentgenograms (Figure 1-2). This apparatus for restitution was of the same size as the roentgen apparatus. The apex of the cones corresponds to the foci, the roentgen rays are materialized by threads, and the roentgen films can be mounted in positions

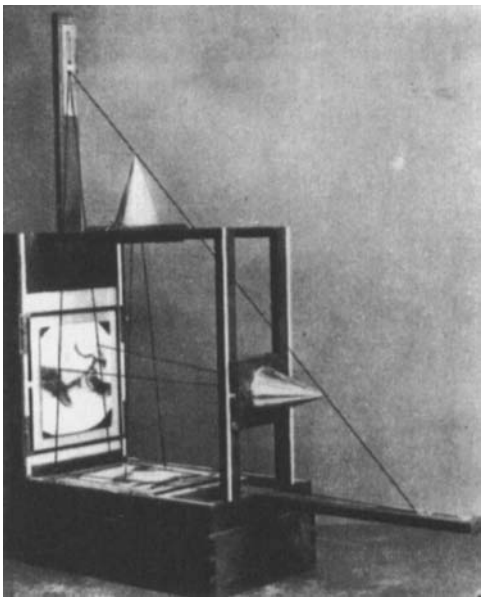

Figure 1-2. Piazzolla-Beloch's restitution apparatus

exactly corresponding to those they had at exposure.

Both Davidson's apparatus and that of Piazzolla-Beloch appear to have experienced little practical use after their original conception. The author is not aware of any publication describing the application of Piazzolla-Beloch's apparatus for any practical purpose.

One problem, when stereoscopic vision is not used, is the identification of corresponding points in a pair of images. Stereoscopic vision, which facilitates the construction of a mental image of the original object, obviously facilitates the identification of object points.

The original mirror stereoscope of Wheatstone (1838) consisted of two plane mirrors, the backs of which are at right angles to each other. The mirrors are vertical, and in roentgen stereoscopy the films are hung so that the left mirror reflects the film exposed from the left position of the roentgen tube, and vice versa for the right mirror. The virtual image is seen in front of the observer, and if the mirrors are transparent, he can move a real object and see it in the virtual stereoscopic image. Hasselwander (1915, 1954) and Trendelenburg (1917) used Wheatstone's stereoscope in this way for direct determinations and measurements in the virtual image. The movement of the roentgen focus between exposures must be equal to the actual interpupillary distance of the observer, and the films must be carefully mounted in the stereoscope, etc., circumstances that make high quality measurements difficult to reproduce. Trendelenburg discusses fully in his monograph (1917) the adjustments which are necessary in this type of measurement. He advocates what he calls "Die unmittelbare Messung des Raumbildes". This consists of the direct insertion of a measuring rod, a protractor, etc., into the virtual image, and it is obvious that the image must be obtained congruent to the object to make the method meaningful. Trendelenburg obtained a root mean square value of length errors (the difference between the mean of five roentgenographically measured lengths and the length determined by direct measurement on a cranium) for 15 different distances of 0.5 mm. The largest error was 1.2 mm.

Laying a bar with two projecting measuring marks on the table where a stereoscopic pair of pictures is mounted, one can, by moving the bar and adjusting the distance between the marks, cause the marks to coincide with the two images of an object point. If the observer views the pair of images stereoscopically, the two marks are perceived as one measuring mark, and the mark is seen floating on the object point on which it was focussed. Depths in the reconstructed object can be calculated from the distance between the marks. Hallert (1960, p. 66) discusses more fully the principle of the floating mark, first conceived by Stoltze in 1892.

Marie and Ribaut were the first to apply the principle of the floating mark to measuring depths in roentgen stereoscopic image-pairs. Their first work on this subject dates from 1899. They had in 1897 studied the optimal conditions for perceiving a roentgenographed object with stereoscopy. They mainly discuss the principles and do not account for any actual measurements.

There has been no rapid development of roentgen stereophotogrammetry, and in his article in "Encyclopedia of medical radiology", (1967) on roentgen stereo methods, Köhnle comments (p. 220): "Die Röntgenstereoskopie befindet sich jedoch infolge der technischen Fortschritte 'in statu nascendi'. Es handelt sich also darum, die 'Keimungsfähigen' Gedanken der klassischen Röntgenstereoskopie herauszustellen, um sie der Entwicklung durch die zeitgemässe Technik freizugeben."

Köhnle uses stereoscopy synonymously with stereo method, and the emphasis of the article is placed on stereoscopes, methods for exchanging the roentgen films rapidly etc. Köhnle himself has taken part in the development of a stereo-comparator for use with stereo photofluorographs (Odelca). Depth values can be read on a numogram in the comparator, if the focus-focus distance (the base) and the screen-focus distance are specified, and the scale for depths is graded in steps of 0.2 mm, which gives a hint of the maximum precision that can be obtained. Other radiologists in Düsseldorf, among them Greul (1968), have supported the development of a stereoscope for the direct evaluation of positions and distances from large-size roentgenograms using the principle of the floating mark as in Köhnle's instrument. Applications have been made, among others, in the field of cephalopelvimetrics. The measuring scale of the stereoscope is graded in half-millimetres, and on a test object (a square box with sides = 100 mm) approximately 93% of lengths measured in a plane parallel to the film show a deviation of less than 0.5 mm. Only 33% of distances in the depth have a deviation less than 0.5 mm.

Later, a commercial roentgen stereo-comparator with generally the same accuracy has been produced by the Zeiss Company, Oberkochen (Meier, 1971).

The instruments described represent a further development and refinement of already well-established principles, introducing among other things, electronic computations of the model

coordinates from the image coordinates and photogrammetric formulas, when the stereoscopic evaluation apparatus is supplied with the focus-focus and film-focus distances.

The development of roentgen stereophotogrammetry in the United States has been remarkably slow, and little influenced by the progress made in Germany. Utilizing a mirror stereoscope and a parallax bar Singh (1970) obtained a quality in depth measurements on a test object approximately equal to that attained by the German investigators. Others discuss special applications. McNeil (1966) mounted the object, a calibration device and the film on a platform, which was rotated between the exposures, thus giving a double image from a single focus. Nicholls et al. (1972) obtained an accuracy of the magnitude of 25 µm when determining positions of lead foil markers on teeth. The dental film was fixed in a holder defining the laboratory coordinate system, and the position of the focus in relation to the film was computed in a separate calibration procedure. The object was than imaged from three different positions of the roentgen focus, obtained by rotating the roentgen tube.

Important achievements in analytic photogrammetry have been made since about 1950 by the late Bertil Hallert and co-workers at the Royal Institute of Technology in Stockholm. Hallert and members in the group have developed methods for the determination of the elements of the interior orientation of photogrammetric instruments. The interior orientation includes the position of the projection centre in relation to the image, and the distortion of the bundle of rays that form the image (Hallert, 1960, p. 18). Utilizing a plane grid, Hallert (1954-1955) developed a method for determining the distortion of a bundle of rays. This method was used by Hollender (1964) to show that there is no systematic deviation from the ideal bundle of rays in roentgenography. Hollender determined the focus-film distance by using a three-dimensional test device and similar triangles. He further showed that a high precision and accuracy, of a magnitude of ten to fifty micrometres, can be obtained in standard roentgenography.

General photogrammetric principles and their applications in roentgen photogrammetry are discussed in a monograph by Hallert (1970).

Torlegård (1967) developed a technique for the determination of the interior orientation of cameras, utilizing a three-dimensional test object, in which the camera is in principle calibrated for each exposure, using predetermined coordinates of the test object.

Such methods, which uses a "calibration cage" have been applied in roentgen photogrammetry, in the works of Patel (1973) and Hindmarsh (1973). In Patel's work, the accuracy of the method was, as he demonstrated it, of the magnitude of about 50 µm.

For a comprehensive review of the use of stereophotogrammetry in medicine, see Herron (1972).

Remarks on the history of the kinematics of rigid bodies

Newton (1643-1727) is the father of analytic mechanics, but his most important studies were on the mechanics of mass-points, and it is from Euler (1707-1783) that the fundamental theorems of the motion of bodies with extension in space emanate.

The kinematics (or the geometrical part of the motion) of rigid bodies are dealt with by Euler in the work "Formulae generales pro translatione quacunque corporum rigidorum", published in 1776 in the proceedings of the St. Petersburg Academy. The word "translatione", as used here, means displacement, including both rotation and translation. Three points deserve special mention.

In paragraph 10 of the cited work, the general relations between the coordinates of a rigid body before (p, q, r) and after a movement (x, y, z) are revealed. Three constants f, g, h determine the translation, nine constants F,..., H" determine the rotation, and the relation is:

$$x = f + Fp + F'q + F''r$$
$$y = g + Gp + G'q + G''r$$
$$z = h + Hp + H'q + H''r$$

In paragraph 13, the nine constants F,..., H" are shown to be functions of three angles, which have been called "the Eulerian angles". It must be noted, however, that no specific choice of these angles is made here, it is only stated that the components of the matrix are functions of three parameters. This fact is derived from orthonormality relations for the coefficients F,..., H".

Paragraph 24 discusses whether, when a rigid body moves from one position to another, there exists a line in the body such that its direction is not changed between the two positions. The existence of such a line is, in the next paragraph, proved for the general motion, with one fixed point in the body. Euler has thus proved, that the general motion of a rigid body with one fixed point, is equivalent to a rotation about an axis through this point.

The generalization of this last theorem, to the case where the body is free to move in space, is obvious. The general free motion of a rigid body is the sum of the translation of an arbitrarily chosen base point, and a rotation about an axis through this point (the rotation axis in Euler's theorem). Different chosen base points will yield different translations (this will be fully discussed in Chapter 6), and the question is whether the choice of a base point can be wisely made.

Cauchy (1827) proved that the general infinitesimal motion of a rigid body can be represented by a rotation about, and a translation along, one and the same axis, and Chasles (1830) proved the corresponding theorem for finite motions. Chasles proved that, for every motion, a base point can be found such that its translation is parallel with the rotation axis, and the movement of the body is, thus represented, nothing more than the motion of a bolt on its' nut ("d'une vis dans son écrou"). Rodrigues (1840) studied various aspects of rigid-body kinematics in terms of this screw motion, and stressed that the translation along the screw axis is the least of possible displacements for a point, moving with the body. He developed a formula for the determination of screw motion parameters from the positions of three points, not on a line, before and after the motion.

Biomechanical studies of the kinematics of skeletal segments, treated as rigid bodies

The Germans Braune and Fischer have a high rank among the fathers of exact, calculative biomechanics. Their earliest joint work (1885) first dealt with a basic discussion of the methods for an exact investigation of the motion of skeletal segments, treated as rigid bodies. It is here pointed out that the most important thing in the study of the motion is to study the motion of the segment itself, not the motion of a certain point in the segment: "Die Wichtigste Frage aber bei der Bewegung eines starren Massensystems ist die Analyse der Bewegung das ganzen Systems übarhaupt." To study the motion of the rigid body, it is sufficient to determine the motion of three points, attached to the body, which are not on a line. The screw motion can then be calculated. By direct measurements they determined the indicators, attached to the radius or ulna during the motion of an arm of a specimen. The measurements were made in a laboratory coordinate system, two axes of which were defined by a horizontal millimetre paper. The position on the third axis was determined on a plumb line from the point to be measured to the horizontal paper. Braune and Fischer would thus seem to be the first in the history of biomechanics to determine true three-dimensional coordinates during the movement of an object, and that in a way allowing determination of the rigid-body motion of the object studied. However, they did not utilize their information for the calculation of the rigid-body motion, but were content with a graphical construction of the position of the screw axis. This is easily explained by the burdens on the computational side posed by a determination of rigid-body motion parameters from measured positions of points.

Later on, in the monumental work "Der Gang des Menschen", the first part of which was published in 1895, Braune and Fischer utilized photogrammetry to determine positions in space of markers (Geissler tubes) on individuals whose walking was studied. They determined the positions in space by numerical intersection of rays, reconstructed from photographs obtained from four cameras with convergent camera directions (60°). The photographs were measured in a coordinatograph with a setting accuracy of 1 μm, especially constructed for their investigations .

The project of Braune and Fischer was extremely time consuming, and demanded the uttermost efforts of the investigators, facts that might explain why projects of this nature were not undertaken until modern techniques had facilitated the tasks of measurement and data reduction.

More than 50 years later, Carl Hirsch and co-workers studied various aspects of joint structure and joint motion, first in the Biomechanics Laboratory of the University of Gothenburg and later in Stockholm, or at their home universities. Lysell (1969) was the first in the group to use a roentgen stereophotogrammetric technique for the study of joint motion (in cervical spine) from three-dimensional determinations of marker positions. His photogrammetric method uses one fixed focus, and a rotation of the object and film, together, between the two exposures. The description of the pattern of motion partly uses a special terminology, rather than the general concepts we have discussed. White (1969) utilized the same photogrammetric method to study the thoracic spine, but he analyzed the motion between two vertebrae in terms of screw axis displacement.

2. A roentgen stereophotogrammetric method

Terminology and introduction

Photogrammetry means, in direct translation, to measure a picture obtained by light. *Stereo* is the property of being solid, having three dimensions. Stereophotogrammetry refers thus to measurements in pictures that make it possible to reconstruct a three-dimensional object from two-dimensional images. It should be noted that stereo means properties of the reconstructed object, and not that stereoscopy, i.e. three-dimensional viewing, is necessarily used in the reconstruction task. As will be seen, we do not use stereoscopy, though other systems for stereophotogrammetric evaluation do so, as was discussed in the review of the literature.

Whether the image to be measured is obtained by visible light or by roentgen rays does not, in principle, change the measuring process or the models for the reconstruction. Techniques developed for camera photogrammetry can be and have been transferred to roentgen photogrammetry.

We shall here present a new method for three-dimensional analytic reconstruction of distinct points of an object, specially adapted for roentgenography.

The projective transformation

Fundamental to photogrammetry is the geometrical law by which an object is transformed to an image on the film. The image-formation takes place by rays from a point, the projection (perspective) centre, through the object to the corresponding point on the film. As the projection is from a centre, it is called a central projection.

Using roentgen rays, the projection centre is the focal spot of the roentgen tube. In camera photogrammetry, we have to correct for the rays being deflected in passing through the lens. In roentgen photogrammetry we can, however, regard the projection as a strict central projection by straight rays, for roentgen rays are not deflected to any appreciable amount when passing through the object, as will be shown later on in this chapter. Hollender (1964) has shown that no systematic distortion of the ideal bundle of rays from the roentgen focus exists, as was discussed in the review of the literature. The law governing the correspondence between object and image is, thus, a strict mathematical central projection.

The formula, connecting coordinates in the object and coordinates in the image is, when both object and image are planes:

$$x = \frac{a_1 x' + b_1 y' + d_1}{a_4 x' + b_4 y' + 1} \qquad (2:1)$$

$$y = \frac{a_2 x' + b_2 y' + d_2}{a_4 x' + b_4 y' + 1}$$

$$x = f_1(x', y')$$

$$y = f_2(x', y')$$

The transformation functions f_1 and f_2 are fractional linear expressions with identical denominators (i.e. Hallert, 1970, p. 40). Here x, y are coordinates for a point in a coordinate system in the object, and x', y' are the coordinates of the corresponding image-point, given in a coordinate system in the film. The coordinate systems may be arbitrarily situated, both in object and image, and may be a general rectilinear coordinate system.

Formula 2:1 contains eight parameters (a_1, b_1, d_1, a_2, b_2, d_2, a_4, b_4) determining the projective transformation. If we determine the coordinates of four corresponding points in object and image, we can determine these coefficients, and thus the transformation. The only restriction on the points is that three of them must not lie on a line (Fishback, 1962, p. 137).

We have now come to a fundamental procedure in our photogrammetric method.

Procedure: Roentgenograph a calibration plane, to which is attached a coordinate system defined by indicators in this plane, together with the object under investigation. Measure the images of the points of the calibration plane and the object points. The image coordinates of the points of the calibration plane, together with their given values in the laboratory coordinate system, determines the transformations f_1 and f_2 from the image coordinate system to the laboratory coordinate system.

Applying this transformation to object points we obtain the intersection between the rays, from the projection centre through the object points, and the calibration plane. We obtain these intersections in the coordinate system of the calibration plane, and have thus transformed image coordinates to positions in the laboratory coordinate system (Figure 2-1).

Terminology: We call the points in the plane used for determining the central projection "fiducial marks". The plane, earlier called a calibration plane, will be called the "plane of the fiducial marks". The term "fiducial mark" is also used in camera photogrammetry. In a camera, the fiducial marks define the position of the perpendicular from the projection centre to the film. The fiducial marks thus have a more extensive role in our method than in camera photogrammetry. The fiducial marks are used in both our method and in camera photogrammetry, however, for determining the relation between the film and the laboratory or camera coordinate system, a similarity which justifies the use of the same term.

Affine deformation: An affine deformation of the film (stretching or shrinkage, temperature expansion) does not influence the procedure above. The affine deformation is mathematically defined by a linear relation:

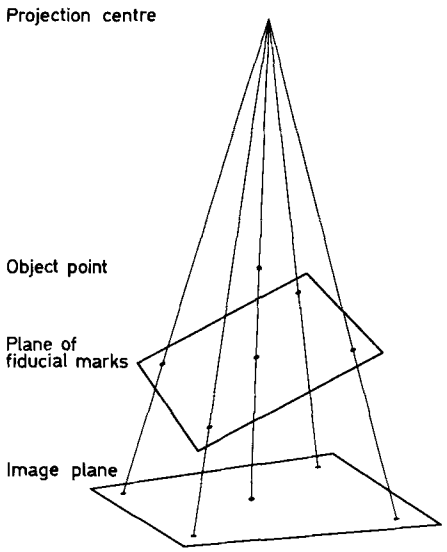

Figure 2-1. A central projection of points in a calibration plane (= the plane of fiducial marks) to an image plane. The intersection of a ray from the projection center through an object point with the plane of fiducial marks is shown.

$$x'' = a_{11}x' + a_{12}y' + a_{13} \qquad (2:2)$$
$$y'' = a_{21}x' + a_{22}y' + a_{23}$$

between the image coordinates x', y' and x", y" before and after the deformation. Inserting either the deformed or the true coordinates in Eq. 2:1, we have a projective relation between the image coordinates and the given coordinates of the fiducial marks, which shows that the result of the transformation to the plane of fiducial marks will not be influenced by an affine deformation.

Technical considerations on the determination of projective transformation. The test cage

The fiducial marks used for determining the projection must form a mathematical plane, something which in practical cases only can be realised to a certain degree. The film must also form a plane. For the further determination of the position of the roentgen focus, we need another plate with indicators, and the plate with the fiducial marks is combined with this second plate to form a rigid body. We have two types of these assemblages, Models 1 and 2, where we have two further minor modifications of Model 1. We have chosen to call the assemblage a test (or calibration) "cage", and speak of "Test Cage Models 1A, 1B and 2" (Figure 2-2).

In Test Cage Model 1 we have one plate with fiducial marks common to the two images that are to be formed from the object. In Test Cage Model 2 we have two plates with fiducial marks, one for each film to be exposed, and the two plates are perpendicular to each other. For Test Cages IA and 2, the film is placed as near the plate as possible, and if we use films, packed in envelopes, these are pressed against it.

Two types of test cages (1A and 2) have been made of Plexiglas plates. They are not very flat. For the sizes we utilize (plates 240 x 210 x 10 mm and 300 x 250 x 10 mm, respectively), the variation in thickness of the plates can be as much as 0.2 mm. This is no direct expression for the lack of flatness, the plate might be equally thick but bent, and it might be unequally thick, for example wedge-shaped, and its surfaces perfectly plane. There are

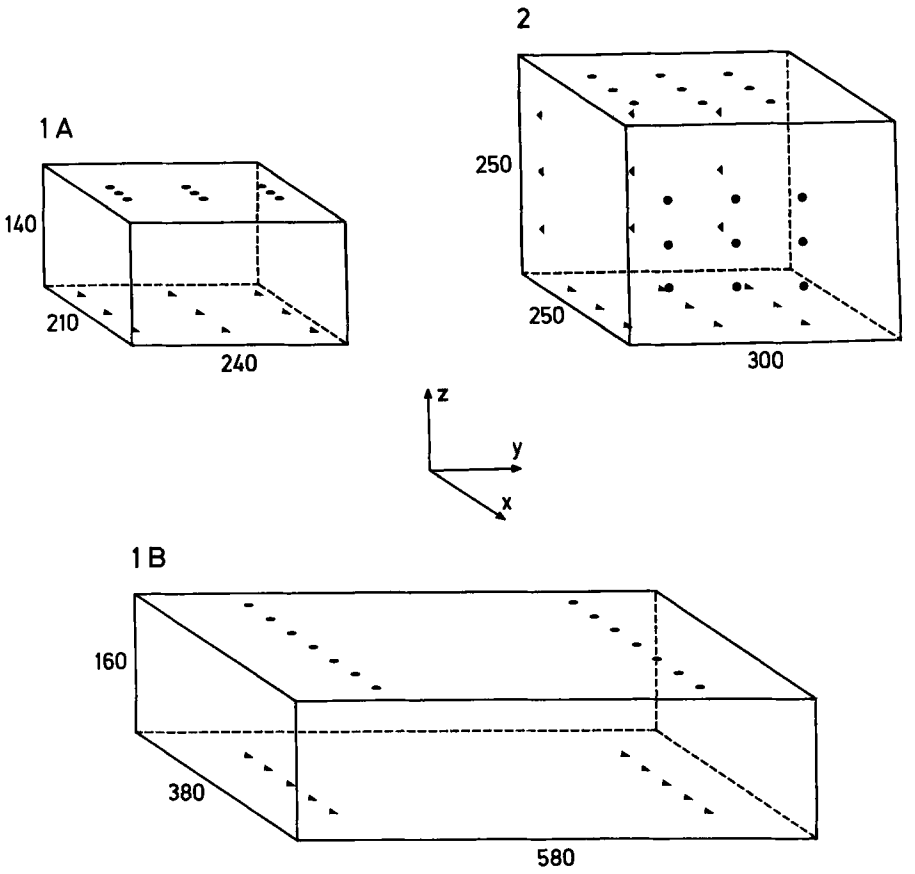

Figure 2-2. The three models of test cages, Models 1A, 1B and 2. The triangles indicate the fiducial marks, and the round dots indicate control points. The laboratory coordinate system (directions of axes shown in the figure), has its origin in the middle proximal fiducial mark of each test cage. In utilizations, the roentgen foci lie approximately in a xz-plane through the center of each cage. Unit: mm.

instruments (special microscopes for instance) to measure the lack of flatness of a plate.

This has been discussed by Hallert (1960 b) and Hollender (1964). As it would be almost impossible to grind a Plexiglas plate in order to obtain flatness, we have refrained from studying this aspect, and possibly compensate for it, so that errors due to the lack of flatness will be included with the irregular errors. In arranging the indicators that constitute the fiducial marks we have fixed the Plexiglas plate to a flat machine bench and cut the indentations for the indicators to an equal distance from this metal bench plate. This will to a certain degree compensate for the lack of flatness of the Plexiglas.

As indicators, we utilize pointed tantalum pins or tantalum balls, both 0.5 mm in diameter.

In the two types of Plexiglas test cages, 1A and 2, there are nine fiducial marks for every film and they form a rectangle having the dimensions 130 x 200 mm. Three marks are placed on each short and each long side, so that the corner indicators are common, and one indicator is placed in the middle of the rectangle (Figures 2-3 and 2-4).

The third type of cage, Model 1B, is intended for larger objects, and for a special variant of our method, in which we separately reproduce the calibration indicators and, also separately, the object on the film. Here we want to get a free area on the film for roentgenographing the object. To obtain this we mask the central area of the cage, and place the indicators on two lines, one proximal and one distal to the masking. In actual constructions, we have had distances of 400 and 420 mm between the lines, respectively, as the opening angle of the roentgen tube has not allowed wider spacing. (The maximal attainable focus-cage distance was 1100 mm). The

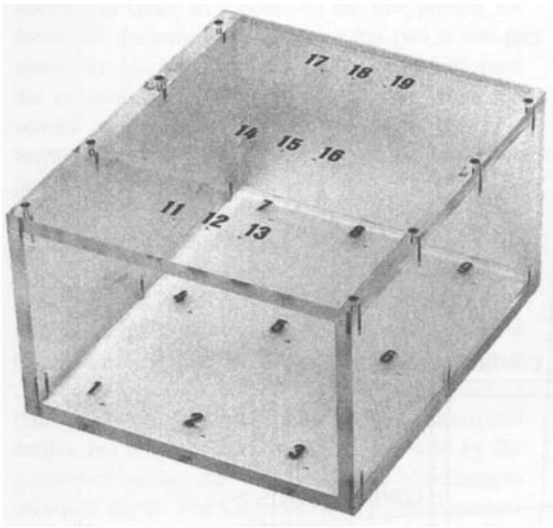

Figure 2-3. Test Cage 1A. Indicators marked with one figure (1-9) are fiducial marks, and indicators marked with two figures (11-19) are control points. The plate with fiducial marks is attached to the plate with control points by two side-pieces. The film is to be placed immediately below the fiducial marks.

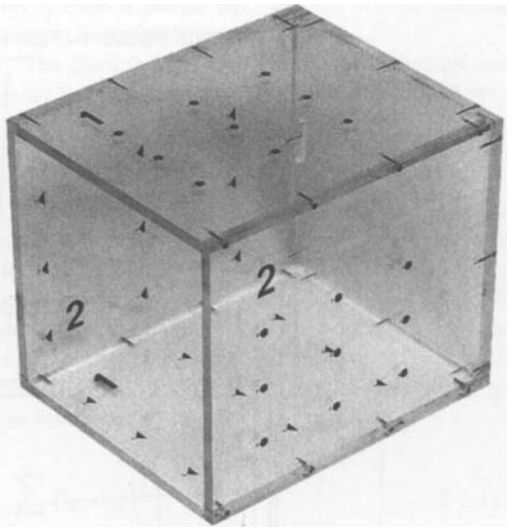

Figure 2-4. Test Cage Model 2. The triangles indicate the fiducial marks, and the round dots indicate the control points. Numbers 1 and 2 indicate the pair of plates for each bundle of rays from focus 1 and focus 2. The films are to be placed below (1) or behind (2) the fiducial marks.

plates of these larger test cages, (Model 1B; Figures 2-2 and 2-5) are made of mirror glass, 6 mm thick, and the indicators are glued with Araldite (Ciba) or Super-Epoxy (AB Plastic Padding, Gothenburg) on the inner surface of the plates. We have five fiducial marks, spaced over a distance of 200 mm, on each of the short sides. As indicators we here use tantalum balls, 0.5 or 0.8 mm in diameter.

Plexiglas has a coefficient of thermal expansion of approximately 75 x 10^{-6}/°C, so that the 200 mm distance between the rows of fiducial marks in a test cage of type 1A is changed 15 µm for every degree of temperature change. We have not been able to obtain the coefficient of expansion of Plexiglas for changes of relative humidity, but swelling might deform the Plexiglas. The plates of Plexiglas are, as mentioned earlier, not very flat. Owing to these circumstances, we will in the future also manufacture the Test Cages 1A from mirror glass (coefficient of thermal expansion about 8 x 10^{-6}/°C).

Determination of the position of the roentgen focus

The laboratory coordinate system: A laboratory coordinate system is determined by the plane of fiducial marks. The origin of the laboratory coordinate system is one of the fiducial marks (the

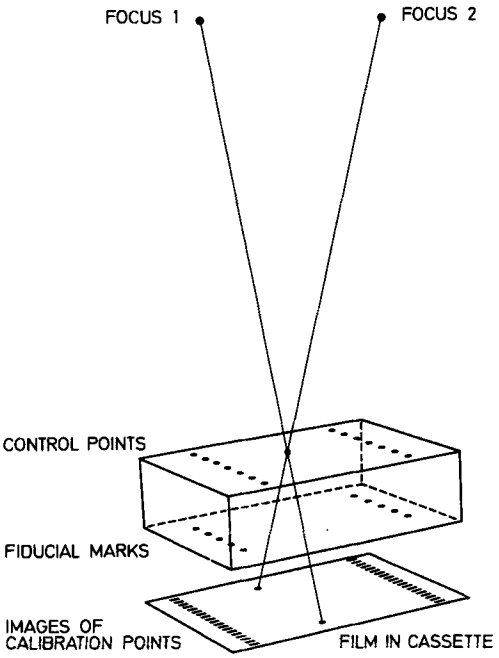

Figure 2-5. Schematic presentation of the set-up when utilizing a test cage of Model 1B. The two zones of images of calibration points (striped in the figure) and the images of an object point are shown.

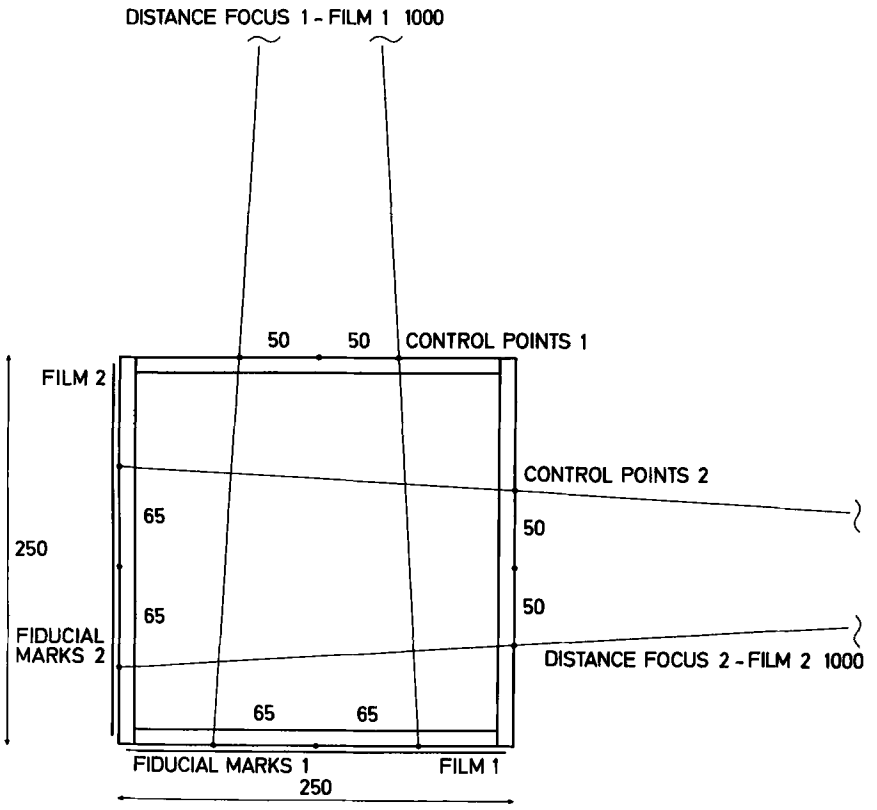

Figures 2-6. A schematic cross-section of a test cage of Model 2, also depicting the course of rays from the two roentgen foci. The section is an xz-plane. Unit: mm.

middle one of the marks in the proximal row), the y-axis goes from this mark to its opposite mark in the distal row, and the x-axis is to the right, orthogonal to the y-axis. The z-axis is perpendicular to the xy-plane, positively directed in the right-handed sense, and thus points towards the roentgen foci. The y-axis is the longitudinal axis of the cage. For Cage Model 2, where we have two planes of fiducial marks, we choose one (indexed 1) to determine the laboratory coordinate system. Our choice of coordinate axes follows international photogrammetric standards (Schwidefsky, 1963, p. 36).

The task is to determine the positions of the roentgen foci in this laboratory coordinate system. The rotating anode is enclosed, which makes it difficult to measure directly on it, and the roentgen tube is supported by stands, which do not permit very exact positioning in space. We also have different arrangements of the tubes for different examinations. In short, to directly determine the positions of the foci is not practical with the roentgen apparatus stands that are in general use. An indirect determination from the roentgenogram is ideal, and this we are able to accomplish. We proceed as follows, and utilize the earlier mentioned second plate of the test cage. In this second plate we have indicators, which we call "control points", with predetermined coordinates in the laboratory coordinate system. How we determine the coordinates of both fiducial marks and control points in one common coordinate system is discussed in the next chapter: "Calibration of the test cages".

On the roentgen film we get the image of the control points. The image is formed by a central projection from the roentgen focus, and the ray from the focus through a control point passes through the plane of the fiducial marks before it impinges on the film. Through the projective transformation, we compute the intersection of the ray with the plane of the fiducial marks. For a certain control point we now have, 1) its position in space, and 2) the

position in space of a point on the line joining the focus and the control point. Knowing two points in space, we can construct the line joining them (and the extension of this line), and as these different control points form a bundle of rays with the roentgen focus as its centre, we can construct the position of the roentgen focus in space.

Technical considerations: Most considerations on the realization of a plane with fiducial marks can be referred to the discussion of the positioning of control points. We have aimed at having a plane of control points, and a plane parallel to the plane of the fiducial marks. In Cage Models 1A and 2 (Plexiglas cages) we have the problem of the lack of flatness of the Plexiglas plates, as was discussed earlier, but it is to a certain degree overwon by the method of cutting the indentations for indicators to an equal depth. For Cage Model 1B, the tantalum control points are glued on the mirror glass surface and should readily form a plane.

To ensure parallelism between the plate of fiducial marks and the plate of control points, they are attached to each other by two plates of Plexiglas, cut together in one operation to guarantee the best equality in height (Figure 2-3). In Test Cage Model 2 we have no side-pieces, but the second set of plates with fiducial marks and the plate with control points are perpendicular to the first set, and they fix and support each other.

We generally use nine control points to determine each focus. In Test Cage Model 1A, all nine points are common to the determination of both foci, but in Test Cage Model 2, we, of course, have separate clusters of control points for each focus. In Test Cage Model 1B, we both have control points lying near the longitudinal axis of the cage, which are reproduced by both foci, and less centrally placed control points reproduced by only one focus.

Utilizing a test cage of Model 1B and a test cage of Model 2, the course of the rays is shown in Figures 2-5 and 2-6, respectively.

Mathematical considerations: The equation of a straight line passing through points P and P_0 with position vectors $\bar{r}_P$ and $\bar{r}_{P0}$ is (Chapter 8):

$$\bar{r} = \bar{r}_P + t(\bar{r}_P - \bar{r}_{P0}) \qquad -\infty < t < +\infty \qquad (2 : 3)$$

If we denote the control points C_υ and denote the position of the image of C_υ in the plane of the fiducial marks as $C_{0\upsilon}$, the bundle of rays through the control points and the focus can be expressed:

$$\bar{r}_\upsilon = \bar{r}_{C\upsilon} + t(\bar{r}_{C\upsilon} - \bar{r}_{0\upsilon}) \qquad \upsilon = 1, \ldots, n$$

for n control points. ($\bar{r}_{C\upsilon}$ and $\bar{r}_{0\upsilon}$ are the position vectors from the origin to C_υ and $C_{0\upsilon}$.)

The lines, which theoretically pass through one point F, the centre of the focal spot, determined by:

$$\bar{r}_1 = \bar{r}_2 = \ldots = \bar{r}_n$$

(the common point of all lines), do not in actual cases intersect due to measuring errors, among other factors. We then search for the best correspondence to the real focus, knowing the lines $\bar{r}_\upsilon$. We determine the point F in space, which has the least sum of squared distances to the given lines. Denoting the position vector of this point F by $\bar{r}_F$, we minimize the sum:

$$\sum_{\upsilon=1}^{n} (\bar{r}_F - \bar{r}_\upsilon)^2 \qquad (2 : 4)$$

where $\bar{r}_F$ varies over all space. The scalar product of two vectors (Chapter 8) is used in Eq. 2:4. The point F thus obtained is our determination of the focus position.

Determination of object coordinates

After having established the projective transformation, we utilize the transformation functions determined to map the image onto the plane of the fiducial marks. We now have the image coordinates transformed into a laboratory coordinate system, and we also have determined the positions of the roentgen foci in this same coordinate system. A certain object point is lying on the straight line joining focus and the transformed image of the point in the plane of the fiducial marks. Knowing these lines for two foci (or more), the position of the object point can be constructed as the intersection of the lines.

We first transform the positions of object points in the films to positions in the laboratory coordinate system, and then construct lines between the two foci and corresponding image points.

We denote the two foci by F_1 and F_2, where we have established the common principle of denoting the left focus, as seen in the positive direction of the longitudinal axis of the test cage, by Index 1. The position vector of an image from the respective focus is indexed with the focus number. The position $\bar{r}_P$ in space of a point P, being simultaneously on the two projection rays, is determined by:

$$\bar{r}_{P1} = \bar{r}_{F1} + t_1 (\bar{r}_{F1} - \bar{r}_{01})$$

$$\bar{r}_{P2} = \bar{r}_{F2} + t_2 (\bar{r}_{F2} - \bar{r}_{02})$$

$$\bar{r}_P = \bar{r}_{P1} = \bar{r}_{P2}$$

$\bar{r}_{P1}$ = position on the ray through Focus 1 with focus position vector $\bar{r}_{F1}$ and image position vector $\bar{r}_{01}$, and the corresponding for Focus 2. First t_1 and t_2 are determined as the unknown quantities of the (three) equations:

$$\bar{r}_{P1} = \bar{r}_{P2}$$

and then the position of P is found after insertion of either t_1 or t_2 in the expression for $\bar{r}_{P1}$ or $\bar{r}_{P2}$.

In reality, the lines $\bar{r}_{P1}$ and $\bar{r}_{P2}$ do not intersect, but pass each other at a certain distance. In the determination of focus, we utilized a computer programme routine that computed the point in space having, in a specified sense, the shortest distance to a number of given lines.

The best corresponding point to an object point P should be the point in space that has the least sum of squared distances to the two lines $\bar{r}_{P1}$ and $\bar{r}_{P2}$, and we also compute the object point in this way. A slight consideration makes it evident that this point is the middle point of the shortest line joining the two projection rays.

The shortest joining line is obviously perpendicular to the two projection rays. As the two rays from foci F_1 and F_2 do not intersect, we say that they cross each other. We compute: 1) the (shortest) distance between the crossing lines, and 2) the vector from the point of Ray 1 to the point of Ray 2 that are closest to each other. This will be discussed more fully in the description of the computer program X-RAY.

The reconstructed object points form a model of the real object.

The size of the focal spot

The roentgen tubes we have utilized are two standard tubes, Siemens Bi125/20/50S. All exposures have been made with the smaller focus.

The focal spots have been measured from their images in a pin-hole camera, and have been found to be squares with sides of approximately 0.7 mm. The focal spot, which showed the more pronounced double-peak intensity distribution, have given images, showing less precision in the photogrammetric reconstruction (Chapter 4, Focus F_1 in our set-ups).

Writers on roentgen stereo-methods (e.g. Köhnle, 1967, p. 262) have stated that the size of the focal spot determines the accuracy that is attainable in roentgen photogrammetry, and it is understood that the precision in roentgenograms cannot be "high". We have, utilizing our roentgen tubes, arrived at determinations of points with a precision of about 5 μm (Chapter 5). We have, however, not separately studied the influence of the size of the focal spot on the image precision.

The displacement of the roentgen rays when traversing an object

Are roentgen rays displaced when traversing an object? In the case where the rays pass through a plane-parallel plate, they emerge displaced by an amount d. Using the laws of refraction, this displacement d can be expressed as a function of the angle of incidence ϕ, the thickness of the plate h, and the refractive indices of the plate, and the surrounding medium, n' and n, respectively:

$$d = h \sin\phi \left(1 - \frac{n \cos\phi}{n' \cos\phi'} \right)$$

$$n \sin\phi = n' \sin\phi'$$

(Jenkins-White, 1950, p. 23). For a number of spectral lines of roentgen rays, Siegbahn (1925) has found the difference δ of the refractive index from 1 to be of the magnitude of 10^{-5}, when the roentgen rays were refracted by a glass prism. Inserting $n' = 1 + \delta$ (the glass plate), $n = 1$ (refractive index of air) in the equations above, an expansion in a geometrical series neglecting quadratic and higher-order terms of δ, will yield:

$$d = \delta h \sin\phi \left(1 + \frac{\sin^2\phi}{\cos^2\phi} \right)$$

For a glass plate with thickness h = 10 mm we see that the displacement of the roentgen rays is of the order of 0.1 μm.

3. Calibration of test cages

Calibration of markers in a plane

Fundamental to our photogrammetric method is, that we have a radiolucent object, with predetermined positions for radiopaque markers. We arrange the markers in this object, the test cage, in planes, and assume that in constructing the test cage, we can reach a parallelism between the planes, corresponding to one focus. To determine coordinates of markers in a plane is an easy task, provided that a rectangular coordinatograph is available. The problem is to determine the position of one plane in relation to another. We shall here describe the calibration of a test cage to the extent it is performed in our investigation.

We start by measuring the plane coordinates of each plate forming the cage. When the size of the field of fiducial marks and the field of control points does not exceed 150 x 200 mm, as in the case for the Plexiglas cages, we place the cage plate on one of the film holders of a Wild A8 Autograph to determine its marker coordinates. For the larger fields of markers in the cages of Model 1B, we utilize the drawing table of the Autograph, which is a rectangular coordinatograph, and which can measure planes up to 1000 x 1000 mm. The evaluation apparatus and the precision of the calibration procedure will be discussed in Chapter 5.

A computer program, which we call CALIB2 (two-dimensional calibration), determines the change of the coordinate system from the instrument system to a coordinate system with given origin in the test cage plate, and given direction of axes. The transformation between the two coordinate systems is, after the measured coordinates have been corrected for the actual scale factor of the instrument, a rotation and translation given by

$$x = x' \cos\theta - y' \sin\theta + x_A \qquad (3:1)$$
$$y = x' \sin\theta + y' \cos\theta + y_A$$

where the primed coordinates are the measured ones, the unprimed ones are transformed plate coordinates, and x_A and y_A are constants (compare with Eq. 6:3a). The three unknown values of the transformation (x_A, y_A, and θ) are determined from the measured position of the origin of the plate's coordinate system, and the measured position of a point on the y-axis of the plate.

With the parameters of the transformation thus established, we determine the positions of our indicators in a coordinate system for each plate, with the origin in one indicator, the y-axis parallel to the long axis of the cage and determined by two indicators, and the x-axis perpendicular to the y-axis and in the plane of the indicators.

A translation of the plate of the control points

We calibrate each separate plate of the test cage, in the way just described. We shall now discuss a test cage of Model 1. The upper plate, as a rigid body, has six degrees of freedom relative to the base plate, three translational and three rotational degrees of freedom. We shall treat these two groups separately, and start with the translational degrees of freedom. This means, that we suppose we have the coordinate axes of the two plates parallel to each other, but do not know the position of the origin of the plate of the control points in the laboratory coordinate system, which is defined by the plate of fiducial marks. An approximate position for the origin of the control points can, of course, be obtained by simple means, as the plates and side-pieces are mounted with reasonable care, and the indicators are positioned on reasonably well-determined distances from the edges. Using this preliminary determination of the position of the plate of the control points, together with the calibration of the separate plates, we say that our test cage is "partially" calibrated, but we can proceed to a "complete" calibration. Within the complete calibration we determine corrections for the preliminary coordinates.

The focus of the roentgen tube is determined as the intersection of lines, from the images of control points, transformed to the plane of the fiducial marks, and through the corresponding control points. We shall now prove the following theorem:

Theorem: If projection lines between images of control points in the plane of fiducial marks and the control points intersect for one position of the plane of the control points, then they will intersect when this plane is arbitrarily translated.

Proof: It is sufficient to prove the theorem for the case with two control points, C_1 and C_2. Their original positions are $\bar{r}_{C1}$ and $\bar{r}_{C2}$, and the positions of their images are $\bar{r}_{01}$ and $\bar{r}_{02}$. The translation of the plane of the control points is $\bar{d}$. As the projection lines intersect before the translation, we have parameters t_1 and t_2 such that

$$\bar{r}_{01} + t_1 (\bar{r}_{C1} - \bar{r}_{01}) = \bar{r}_{02} + t_2 (\bar{r}_{C2} - \bar{r}_{02}) \quad (3:2)$$

If we can find parameters t'_1 and t'_2 such that

$$\bar{r}_{01} + t'_1 (\bar{r}_{C1} + \bar{d} - \bar{r}_{01}) = \bar{r}_{02} + t'_2 (\bar{r}_{C2} + \bar{d} - \bar{r}_{02}) \quad (3:3)$$

we have proved that the projection lines intersect after the translation.

The z-component of Eq. 3:2 is

$$0 + t_1 (z_{C1} - 0) = 0 + t_2 (z_{C2} - 0)$$

as the plane of fiducial marks is the plane $z = 0$. Further, we have $z_{C1} = z_{C2} = z_C$, which shows that $t_1 = t_2 = t$. If we put $t'_1 = t'_2 = t$, we see that Eq. 3:3 becomes Eq. 3:2, which completes the proof of our theorem.

The result, $t_1 = t_2 = t'_1 = t'_2 = t$, can be further utilized. From the z-component of Eq. 3.2 it follows for the z-component of focus coordinates z_F that:

$$z_F = 0 + t (z_C - 0)$$

inserting the value for t, obtained from this equation in Eq. 3.3, we find that the translation $\bar{d}$ leads to a translation $\Delta\bar{F}$ of focus:

$$\Delta\bar{F} = \frac{z_F}{z_C} \bar{d} \quad (3:4)$$

Proceeding analogously, we can show that rays from the computed foci which intersect and thus define a model point, also intersect after we have displaced the foci, as the result of a translation $\bar{d}$ of the plate of the control points. If z_P is the z-coordinate of the model point P, the translation $\Delta\bar{r}_P$ of the model point due to the translation $\bar{d}$ is:

$$\Delta\bar{r}_P = \frac{z_P}{z_C} \bar{d} \quad (3:5)$$

Determining the translational error in positioning the plate of control points

Errors in the determination of the position of the plate of control points will lead to deformations of the model. We have determined (Eq. 3:5) the relationship between the errors in the position of the plate $\Delta\bar{r}_C$ (correspondence to the translation $\bar{d}$) and the model errors $\Delta\bar{r}_P$:

$$\Delta\bar{r}_P = \frac{z_P}{z_C} \Delta\bar{r}_C$$

Measuring model errors determines the translational error in positioning the plate with control points. We shall see how this can be performed even without knowing the object coordinates in advance. We describe the procedure with reference to the following test object:

Test object: Four parallel bars of quartz glass form the long sides of the test object. Pairs of bars form the long sides of a rectangle, and the two rectangles are joined by four vertical glass bars of equal height (Figure 3-1). The two glass rectangles were ground to get a flat surface before they were fused. There are eleven indicators (pins or balls) on each bar, spaced 20 mm from each other, so we have a total of four measuring bars 200 mm in length, with a total of 44 indicators. The vertical distance between the two rectangles is 80 mm, and the horizontal distance between the long sides is 90 mm. The dimensions are determined from the condition, that the test object is to be the largest three-dimensional object to be radiographed in our smallest test cages.

Calibration procedure: Radiograph the test object in two positions, A and B, and eventually in two further control positions, C and D. Attach a coordinate system to the test object, with the origin in one of the proximal indicators in the lower rectangle, let the y-axis be the long axis of the test object and lay the x-axis in the lower plane. The test object has coordinate axes parallel to the axes of the cage in position A. In position B we have rotated the object 180 degrees about the z-axis of the cage. We can then obtain model coordinates of the test object in positions A and B, in this test object coordinate system. The upper rectangle is at height z_h (we: $z_h \approx 80$ mm) in this system.

In position A, the error $\Delta\bar{r}_C$ of the plate of the control points will lead to an error

$$\Delta\bar{r}_{hA} = \frac{z_h}{z_C} \Delta\bar{r}_C$$

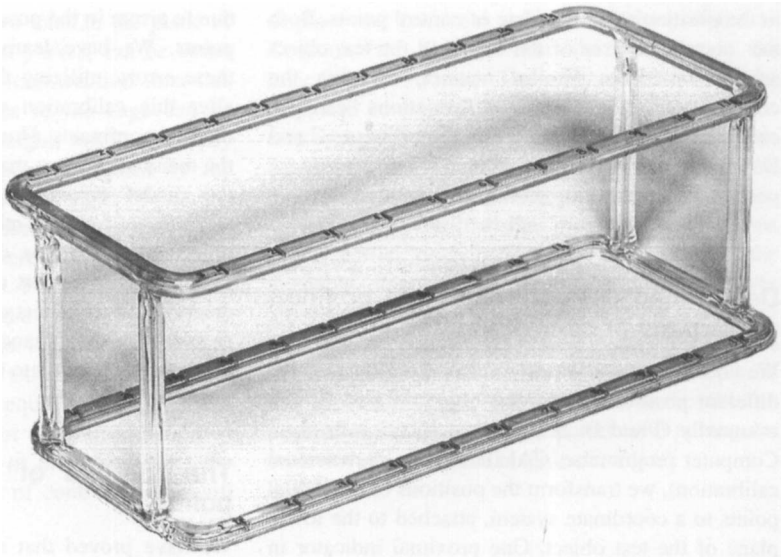

Figure 3-1. The three-dimensional test object. Each of the four horizontal bars contains 11 indicators, with a distance of 20 mm between the indicators. The vertical distance between the upper and lower rectangles is 80 mm, and the horizontal distance between two bars is 90 mm. The 44 indicators are thus spaced over a test area of 200 x 90 x 80 mm.

in the model coordinates of the upper plane. If we know the true object coordinates we thus can compute the error $\Delta\bar{r}_C$ from the determined model coordinates. However, it is not certain that we know the true coordinates, and we then proceed to study the object in position B. Here, the directions of the test object's x- and y-axes are reversed, but the model errors in the test cage coordinate system are the same as in position A. We study only errors in x- and y-directions. Because the directions of these coordinate axes of the test object are reversed, the errors become

$$\Delta\bar{r}_{hB} = -\Delta\bar{r}_{hA}$$

If we compare the test object model in position A and in position B, subtracting the values in A from the values in B, we get the change $\Delta\bar{r}_{AB}$ of the upper plane from A to B

$$\Delta\bar{r}_{AB} = \Delta\bar{r}_{hB} - \Delta\bar{r}_{hA} = -2\frac{z_h}{z_C}\Delta\bar{r}_C \qquad (3:6)$$

This model deformation can be measured without knowing the true object coordinates, and we can determine $\Delta\bar{r}_C$.

$$\Delta\bar{r}_C = -\frac{1}{2}\frac{z_C}{z_h}\Delta\bar{r}_{AB}$$

Note that the correction to the coordinates of the plate of the control points is $-\Delta\bar{r}_C$, thus

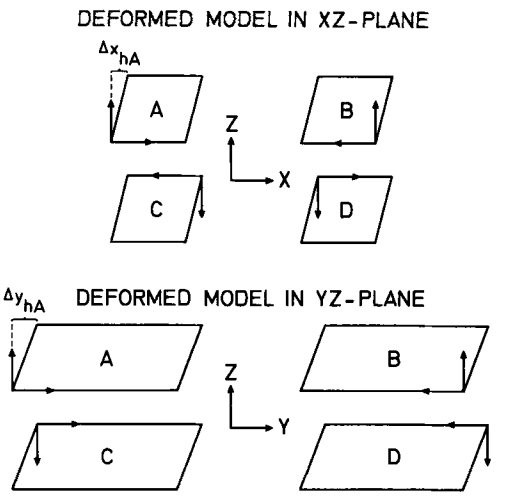

Figure 3-2. Deformation of the model of a three-dimensional test object due to a translation error of the plate of control points. Both the laboratory coordinate system and a coordinate system attached to the test object are shown. The test object is placed in four positions, A, B, C, and D, in the test cage.

$$\text{correction} : \frac{1}{2}\frac{z_C}{z_h}\Delta\bar{r}_{AB} \qquad (3:7)$$

The positions C and D, mentioned above, are obtained after a rotation of the test object 180° about the y-axis, starting with positions A and B, respectively. Figure 3-2 shows the test object from the short and long sides in the respective positions, and how its model is deformed due to a certain error

in the positioning of the plate of control points. Both the coordinate axes of the cage and the test object are shown. In a similar manner, as with the combination AB, model deformations can be computed for combinations with the positions C and D. For example, Δx_{AC} and Δy_{AD} provide a possibility for checking, both being equal to zero.

Determined corrections to the position of the plate of control points

We determine the test object coordinates for different positions of the test object, A and B, and eventually C and D, as described. Then, utilizing a Computer programme, CALIB3, (three-dimensional calibration), we transform the positions of the model points to a coordinate system, attached to the lower plane of the test object. One proximal indicator in this plane defines the origin, the distal one on the same bar defines the direction of the y-axis, and a third indicator on the second lower bar defines, together with the earlier mentioned indicators, the xy-plane. Subtracting the evaluation A from the evaluation B, the vector $\Delta\bar{r}_{AB}$, Eq. 3:6, is determined from the mean x- and y-coordinates of the upper plane in relation to the corresponding coordinates of the lower plane.

Inserting the appropriate values for z_h and z_C, in Formula 3:7, we obtained the corrections (-237, 217) μm and (-41, 44) μm, respectively, for two test cages of Model 1A (z_C = 140 mm). The standard error of the correction, computed from three determinations of Δx_{AC} and Δy_{AD}, respectively, is (32, 8) μm. The fact that the x-value of the standard error is larger than the y-value, can to a certain degree be explained by flexibility of the test cage in the x-direction, which was later corrected.

For two test cages, Model 1B, (z_C = 150 mm), we obtained the corrections (275, 15) μm and (–413, –384) μm. The standard error, determined here from two double-determinations of Δr_{AB}, is (32, 44) μm.

Comment: In test cages, where we have glued the plates with calibration indicators, the positioning of the plates can not be expected to be as precise as when we screw together the different parts of the test cage.

Calibration of the test object

We radiograph the test object in positions A and B, and evaluate the two models in the coordinate system of the object. The two models are deformed due to errors in the position of the plate with control points. We have learned how to compensate for these errors, utilizing the procedure described, and after this calibration we can again calculate the model coordinates. However, it is sufficient to take the mean of the two models A and B, in which way the model errors, $\Delta\bar{r}_{hA}$ and $\Delta\bar{r}_{hB}$, respectively, compensate for each other. The z-coordinates of the object points can be determined more exactly by radiographing the test object from its side. For this determination, the test object is positioned in the test cage so that the distance between the two planes of indicators is parallel to the xy-plane of the cage.

The rotation of the plate of control points

We have proved that a translation of the plate of control points does not influence the intersection of computed lines between control points and their images. A rotation of the plate obviously changes the intersection of these projection lines. The constructed bundle of rays for a given set of image points diverges if coordinates of control points, which are faulty due to a rotation of the plate of control points, are entered in the equations for the projection lines.

We have utilized this to determine the rotation of the plate of control points about a z-axis, perpendicular to the plate (Test Cage Model 1).

If we denote the rotation angle about the z-axis by θ, we will have new x- and y-coordinates (x_r, y_r) after a rotation about the point (x_0, y_0)

$$x_r = x_0 + (x - x_0)\cos\theta - (y - y_0)\sin\theta$$

$$y_r = y_0 + (x - x_0)\sin\theta + (y - y_0)\cos\theta$$

Only the position vector $(x - x_0, y - y_0)$ in relation to the rotation center is to be transformed, and the formulas are completely analogous with Formula 3.1 for the coordinate transformation.

We now vary the angle θ and determine the angle θ for which the sum of squares of distances in Eq. 2:4 is a minimum. We have now two variables to minimize over, the spatial position of focus $\bar{r}_F$ and the angle θ, but a modern high-speed computer handles this easily. It must be noted that the position (x_0, y_0) of the rotation centre does not influence the computed value of θ, as the result of two different choices of rotation center will only differ by a translation of the plate of control points. However, as the center of rotation we always choose the midpoint of the plate of control points.

The rotations about the two axes in the plane of the control points, the x- and y-axes, can be better controlled in the process of construction than this rotation θ, as the side-pieces of the cage can be constructed to be of equal height, but theoretically these rotations could also be investigated by the method described.

The interest of this method is focussed on utilizations of test cages, where we have glued the plates with calibration points. For two test cages of Model 1B, we obtained the rotation angle θ, determined in each case from 10 different films, to 0.111° and 0.001° (mean value), with standard errors of the determination equal to 3.1×10^{-3} and 0.7×10^{-3} degrees. In the first case, the rotation of 0.111° around the midpoint of the line joining the axial indicators of the plane of control points, will displace the proximal indicator 328 μm in the x-direction (the distance from the midpoint to the indicator is 170 mm). The other indicators will be displaced corresponding distances, and entering the rotated coordinates of the control points, we can determine new focus positions and compute new model coordinates of the object.

However, even for the three-dimensional test object earlier described, which fills most of the available object space, no model coordinate was altered more than 4 μm as a result of the rotation of the control points. This seems to show that a determination of the rotation is superfluous, as, in the construction, we might expect to be able to position the plate of control points with an angular error not exceeding the magnitude of 0.1°.

4. The computer program "X-RAY" and examples of its print-out

Introduction. Input and output

The computer program X-RAY is the program system for the photogrammetric part of our investigation. The program is written in FORTRAN for a Univac 1108 computer, working under operating system Exec 8.

The input to the program consists of the measured image coordinates from the roentgenograms and the coordinates of the calibration indicators in the test cages. The output of the program is in the form of punched cards with object coordinates in the coordinate system of the test cage and lists with information on the computational process.

The roentgen film coordinates are recorded during the measurement of the roentgenogram on a five-channel paper tape. For every roentgenogram (or pair of roentgenograms, when we have used a test cage of Model 2) we start a new file on the paper tape by giving the ten-figured time identification number of the roentgen film (year-month-day-hour-minute) and the identification number(s) of the object(s).

After we have focussed the measuring mark in the evaluation apparatus on the image of an indicator, we enter the identification number of the indicator on a control table, and can then record this identification number plus the image coordinates on the paper tape and on a type-writer by pressing a button. In this way the image coordinates are automatically recorded.

The identification number of an image point has two figures for a fiducial mark, three figures for a control point and more than three figures for an object point. (With object point is understood a point not belonging to the test cage.) The three types of points: 1) fiducial marks; 2) control points; and 3) object points can thus easily be assorted by the computer. The last digit of each identification number indicates from which focus the image is formed, and is thus either 1 or 2, for images from focus 1 or 2, respectively. The computer assorts according to this last digit for each stereo roentgenogram, as the two bundles of rays from the two foci will be treated separately up to the last step in the computational procedure.

It is seen from this description of the computational process, that we can not have more than 9 fiducial marks, indicated 11-91 or 12-92, for the image from one focus. This seems to be quite sufficient when using cages of Model 1A or 2, but may be a limitation when using Cage Model 1B. For control points, we have the numbers 111–991 and 112-992 free, which are quite sufficient for all purposes.

The paper tape is played over to magnetic tape at the computer centre, and this tape plus the program's card-deck is the direct input for the following computation.

As was discussed in Chapter 9, the computation proceeds in three steps:

1. Projective transformations from the image to the laboratory coordinate system.
2. A computation of foci coordinates.
3. A computation of object coordinates.

For Step 1, we utilize the fiducial marks, for Step 2, we utilize the control points and for Step 3 we utilize the object points.

We intend to describe how the three successive steps are performed, and what data on the accuracy of the process is printed out.

The projective transformation

Determining the projective transformations, we perform a numerical rectification to the plane(s) of the fiducial marks (Hallert, 1970, p. 40). For each bundle of rays from foci 1 and 2, we determine the eight coefficients in the transformation functions:

$$x = f_1(x', y') \qquad (2:1)$$

$$y = f_2(x', y')$$

We always have nine fiducial marks. From the corresponding positions in the plane of the fiducial marks and the image, we get 18 equations (nine pairs of x- and y-coordinates) for the determination of the 8 coefficients. The number of redundant observations is thus 18-8 = 10, corresponding to five redundant fiducial marks. Using a library sub-routine, GAUSSA, the coefficients of the trans-formation are determined to achieve the best

possible agreement between the given coordinates of the fiducial marks and the corresponding image coordinates in the sense of the least-squares method. We treat the given coordinates as exact, and give equal weight to all the image coordinates. The subroutine GAUSSA (Wedin, 1974) performs successive linear approximations in order to compute the minimum of the sum of squared distances between the given coordinates and transformed image coordinates.

The distance between the transformed image point and the given fiducial mark is the radial error. In the printing-out we give the root mean square of these radial errors, and the maximal radial error for the transformation of each bundle of rays from foci 1 and 2. For the sake of completeness, we also give a table where given and computed coordinates for the fiducial marks are tabulated side by side. The computed coordinates are computed using the determined coefficients of the projective transformation.

To deal with a measurement of a roentgenogram, in which a gross error has arisen in the procedure, we have a subroutine which begins to act when the radial error for a fiducial mark exceeds a predetermined value. This parameter we have generally placed at 250 μm. The subroutine starts by picking out one fiducial mark at a time, when the maximum error exceeds this limit of 250 μm, and running through the nine possible picking-outs, the fiducial mark is disregarded for which the fitting of the remaining ones was the best. The subroutine proceeds with the picking-out till the maximal radial error is less than 250 μm, or only four fiducial marks remain.

This subroutine might be rather superfluous. Isolated gross errors are rare. More common (but still rare in our practice) is the case when one row of fiducial marks has been misread, and in this case too few of the fiducial marks are left to make the evaluation of the picture meaningful. We would recommend reevaluating each picture with a gross error, thus making the subroutine unnecessary.

Using Test Cage Model 1, we have a common plane of the fiducial marks for both bundles of rays, and in all our constructions of Model 1 we have also had identical fiducial marks for the two bundles. This is not needed for computational purposes as the two bundles are treated separately, but gives, of course, a heightened accuracy to the procedure, as we need no calibration between two systems of fiducial marks.

For a test cage of Model 1, the plane of the fiducial marks defines the xy-plane through the origin of the laboratory coordinate system, as discussed earlier, and the transformation to this plane gives coordinates x, y and z = 0 for all three kinds of points. After the coefficients in the perspective transformation are determined, we compute the image coordinates for control points and object points transformed to this plane, and the output of the perspective transformation for Cage Type 1 thus is the vector (x, y, 0) in the laboratory coordinate system for each image point.

Table 1. The root mean square errors (RMSE), the standard errors (SE) and the maximal radial errors for a sample of 10 consecutive perspective transformations. Unit: μm

	Focus 1			Focus 2		
	RMSE	*SE*	Max. error	RMSE	*SE*	Max. error
Cage Model 1A	27	*6.6*	68	21	*4.7*	61
Cage Model 1B	63	*22*	151	56	*15*	112
Cage Model 2	24	*4.5*	52	20	*3.8*	49

Using a Test Cage Model 2 we have two plates with fiducial marks, at right angles to each other. The plate corresponding to focus 1 is the xy-plane with z = 0, and the plate corresponding to focus 2 is thus a yz-plane (constant x-coordinate = $x_{const.}$). The transformation for the bundle of rays from focus 1 thus proceeds as when using Cage Model 1, giving an output vector (x, y, 0), but for the transformation of the bundle from focus 2 we have as output vectors ($x_{const.}$, y, z). In this way the two pictures, from foci 1 and 2, have been transformed to one laboratory coordinate system, with transformed image coordinates in this coordinate system.

Obviously we need a little modification in the structure of the program between the evaluation of a roentgenogram from a cage of Model 1 versus that from a cage of Model 2. The modification, however, is rather superficial and affects only the arrangement of data after the perspective transformation to the two planes. Neither the perspective transformation itself, nor the further calculations after the transformation to the coordinate system of the test cage, will be influenced by the choice of test cage.

Concluding our treatment of the perspective transformation, we give information on the root mean square errors (RMSE), the standard error (=standard deviation) and the maximal radial errors for 10 consecutive transformations, utilizing the different cages, Models 1A, 1B and 2 (Table 1). For Models 1A and 2 we exposed the roentgenograms on industrial film but for Model 1B we utilized film between intensifying screens.

Computation of foci coordinates

In the second and third steps,the image coordinates to be discussed are the coordinates transformed to the plane(s) of the fiducial marks. We can interpret these transformed image points as the intersection of the rays, between foci and object or control points, and the plane(s) of the fiducial marks (Figure 2-1).

Knowing two points on the projection line from the focus, this line is determined, and for each control point and corresponding image point we have a line on which the focus lies. The input to the computer program X-RAY contained cards with the coordinates in the laboratory coordinate system of the test cage indicators. We can thus construct lines through the foci. In Chapter 2, we described the mathematics involved in the determination of foci coordinates from the projection lines. We utilize 8 or 9 projection lines for the determination of each focus. In a Test Cage 1B we have, in contrast to the case with the fiducial marks, not all of the control points common to the two foci. Only two control points on the longitudinal axis are common for the two foci determinations. For a Test Cage Model 2 the control points are separate for each focus.

Besides the printing of the positions in the laboratory coordinate system of foci 1 and 2, we give the following information regarding the quality of the determination of each focus.

1. The root mean square value (RMSV) of the distances between the projection lines and the computed focus.
2. The maximal distance between a projection line and focus.

Further, as complementary information we give tables for:

3. The given coordinates of each control point, and the distance between focus and the projection line through this particular control point.
4. For control points common to both foci, we further give the computed coordinates of this control point, computed using the earlier determined values for foci coordinates.
5. For the control points of Paragraph 4, we further determine the radial errors, the root mean square value of the radial errors, the maximal radial error, the distance between the two lines used for computing the control point, and the root mean square value of these distances.

This is a large amount of information, but only Paragraphs 1 and 2 are of primary interest. The distance between the projection line and focus is analogous to the distance between the fiducial mark and its computed value is expressing how well the respective determinations are achieved. It should be remembered, however, that the projection line extrudes about eight times the distance between the image and the control point to the place where the lines cross, so that errors in the determination of image coordinates will be magnified eight times.

Table 2. The root mean square values (RMSV), the standard errors (SE) and the maximal radial errors for a sample of 10 consecutive computations of foci coordinates. Unit: μm

	Focus 1			Focus 2		
	RMSV	*SE*	Max. dist.	RMSV	*SE*	Max. dist.
Cage Model 1A	424	*150*	1169	316	*138*	898
Cage Model 1B	414	*62*	791	325	*64*	833
Cage Model 2	193	*25*	369	137	*30*	306

Analogous to the way we disregarded fiducial marks giving rise to errors in the determination of the projective transformation above a fixed limit, we discard a control point when the distance between the computed focus and the projection line is above a chosen limit. Proceeding as discussed above, we can set the limit for the highest distance from the focus to a projection line at 2 mm = 8 x 250 μm, if we use the limit 250 μm in rejecting a point for the perspective transformation. As gross errors are rarely experienced in actual practice, we have not had much use for this subroutine for eliminating incorrectly determined control points.

For 10 consecutive computations of foci coordinates, utilizing test cages of Models 1A, 1B and 2, respectively, we have obtained the following quality expressions (Table 2).

Computation of object coordinates

The third step, the computation of object coordinates, is easily carried out when the object image points and the foci are determined in one and the same coordinate system. As was earlier described in Chapter 2, we construct the two lines corresponding to the two images of an object point from the two foci, and then determine the point in space that has the least sum of squared distances to the two projection lines. The point in space thus determined is taken to be the object model-point. We print its coordinates in the data-listing and a card is punched for each object point. The punched card contains 1) the object identification number, 2) the

specific point number in the object, 3) the three-dimensional coordinates of the model-point in the laboratory coordinate system, and 4) the identification time number.

A quality expression much discussed in photogrammetric literature is the distance between the two projection lines to an image point-pair. The shortest line segment joining the two projection lines represents a lack of intersection. We calculate and print this "error" vector, pointing from the projection line from focus 1 to the projection line from focus 2. With our choice of coordinate axes, the error vector points essentially in y-direction, and is in principle the y-parallax of classic photogrammetry (Hallert, 1970, p. 47). We study here only the y-component of the error vector, and for the sake of simplicity call it the y-parallax.

When utilizing a cage of Type 1, the error vector depends, among other things, on 1) precision errors in the measurement of the film and 2) the film's lack of flatness. We can not have systematic errors here depending on faulty calibration between plates of fiducial marks as the fiducial marks are common to the two images, but this circumstance can come in as a systematic error when using a test cage of Type 2. In this cage model, with two separate plates of fiducial marks, an error in the determination of the relative positions of the plates expresses itself in a lack of intersection of projection lines.

We shall first give some information on the error vector in the case of the first cage of Type 1A. For a well-defined object close to the film (the test rod, Chapter 5) with the image of the point of a tantalum pin to focus on, we have computed the y-parallax four successive determinations over the eleven points of the test rod (Table 3).

For the three-dimensional test object (Chapter 3) with tantalum pins, and the corresponding test object with steel balls (0.4 mm in diameter), we have computed values for four determinations of each of the clusters of 44 points (Table 4).

The fact that the mean y-parallax is almost constantly positive may be related to a constant bending of the film, here industrial film packed in envelopes. The influence of bending the film is clearly demonstrated when using a cassette in conjunction with a test cage of Type 1B. We obtain a fairly constant mean y-parallax when laying the cassette on a table, but another one when hanging the cassette on the wall (Table 5).

We conclude that the etiologic factor for the large y-parallax is bending of the cassette. It must be noted that the results for the quality of the photogrammetric procedure demonstrated in the next chapter are achieved with the cassette on the table.

Table 3. The error vector (y-parallax) using Cage Model 1A and a test rod (Chapter 5) with 11 points close to the film in 4 successive determinations. Unit: µm

y-parallax	Determination 1–4			
Mean	5	7	0	0
SE	*11*	*6*	*13*	*7*

Table 4. The error vector (y-parallax) using Cage Model 1A and a three-dimensional test object (Chapter 3) with 44 pins or steel balls in 4 successive determinations. Unit: µm

y-parallax	Tantalum pins				Steel balls			
Mean	7	7	0	5	8	8	3	7
SE	*23*	*19*	*20*	*18*	*19*	*22*	*19*	*18*

Table 5. The error vector (y-parallax) using Cage Model 1B and a cassette on a table or on the wall demonstrating the influence of bending the film. Unit: µm

y-parallax	Cassette on Table				Casette on Wall			
Mean	-234	-345	-203	-261	-22	-44	-29	12
SE	*65*	*70*	*58*	*62*	*56*	*33*	*72*	*38*

Table 6. The error vector (y-parallax) using Cage Model 2 and the 3-D test object with balls and industrial film or film between intensifying screens with a grid . Unit: µm

y-parallax	No grid				Grid			
Mean	-28	-15	-18	-18	-13	-18	-11	-8
SE	*25*	*20*	*22*	*22*	*46*	*26*	*42*	*39*

Finally, we discuss the intersection of projection lines for the first cage of Type 2. The object is again the three-dimensional test object with the balls (diameter 0.4 mm) that we have used in the other investigations.

As the rays strike the films more straightly in this case than in the case with Cage Type 1, the influence of bending of the film ought to be smaller. The systematic part of the parallaxes can be interpreted as error in the relative calibration of the two plates of fiducial marks, and/or the plates of control points.

The precision is, as can be expected, as good as in Cage Type 1A, when we expose on industrial film, but falls off when we use a grid (90 lines/inch) and film between intensifying screens (Table 6).

5. Precision and accuracy of the roentgen stereophotogrammetric method

The evaluation apparatus

For measuring image x'- and y'-coordinates, we utilize an instrument which is commonly employed in cartography, the Wild Autograph A8. For small image sizes, (size of the image about 200 x 150 mm, utilization of Test Cages 1A and 2) we lay the film in one of the film holders. Via an optical system, a measuring mark (a circular dot with a diameter equal to 70 μm) can be focussed on the point to be measured. The image coordinates can then be recorded automatically on a paper tape. The measured coordinates are recorded in units of about 5 μm, varying with the actual adjustment of the instrument.

The instrument was calibrated by the manufacturer before the start of our investigations.

A drawing table is coupled to the main instrument and can be used as a rectangular coordinatograph for images up to 1000 x 1000 mm. On the moving scale, we have attached a small television camera (Sharp, supplied by EMI, Stockholm), mounted so that it magnifies the roentgen film about 15 times. The magnified image is shown in a monitor, and we focus the point to be measured in a circle which has been attached to the centre of the television screen.

Comment: A transmission of the roentgen image by television in the manner described above has proved to be indispensable. It speeds up the measuring procedure, in comparison with use of the microscope on the scale, and by varying the contrast on the screen, measurement on less well-defined points can be more easily facilitated.

When using Test Cage 1B (image size about 700 x 400 mm), we always evaluate the films via the television monitor. The precision in image coordinates, obtained for this kind of measurement, and discussed later on in this chapter, is about 25 μm for each coordinate. This value is obtained when comparing two repeated measurements of each image point, performed with a time interval of more than 1 hour. This shows that there is no large drifting of the central part of the television image. The measured coordinates can be recorded in units of 15 μm for the film sizes we use.

The precision in the calibration of the plates of the test cages

In a calibration of the smaller test cages (Models 1A and 2), we utilize the film holder of the Autograph. When calibrating a test cage of Type 1B, we measure the coordinates of the indicators via the television image from the drawing table of the Autograph, in the same way as when measuring the larger films. Three tantalum pins, placed in the form of a "T" so that their points meet, define a calibration point in smaller cages.

In Test Cage 1B we have tantalum balls (diameter 0.5 or 0.8 mm) as indicators. The coordinates of a calibration point are obtained from five replicated settings. The precision of one setting for the smaller cage is about 10 μm, and about 15 μm for the larger cages (radial errors).

The results from three calibrations of the plane of fiducial marks in a Test Cage 1A is shown in Figure 5-1. The coordinates of the fiducial marks are those in the laboratory coordinate system, after the translation and rotation of the primary measured values have been performed, as described in Chapter 3. The second calibration in the figure has been utilized for investigations with the test cage. Differences between the calibrations can partly be explained as due to faulty control of the calibration temperature.

Irregular errors in measuring image coordinates: The influence of the errors on model coordinates

We shall study the precision in determining image coordinates, and how errors due to lack of precision influence the computed model coordinates.

Hallert (1970, p. 48) deduces expressions connecting errors in image coordinates and errors in the elements of interior orientation with errors in model coordinates. He assumes that the two foci are at an equal height, c, over the films, and studies the influence on model coordinates of errors in this height c, of errors in the distance between the foci, b, (the base), and of errors in the image coordinates. The computations are made by differentiating the formulas for model coordinates in the photogram-

PLANE OF FIDUCIAL MARKS IN A TEST-CAGE MODEL 1A

7	8	9
-65.061, 200.102	0.0, 200.040	65.033, 199.997
-65.056, 200.088	0.0, 200.017	65.022, 199.998
-65.053, 200.063	0.0, 200.008	65.032, 199.978

UPPER LINE 1972-10-23 23.8°C
MIDDLE LINE 1972-10-28 23.5°C
LOWER LINE 1973-05-09 23.4°C

4	5	6
-65.032, 100.055	-0.003, 100.003	65.021, 100.029
-65.032, 100.040	-0.003, 99.992	65.007, 100.013
-65.031, 100.045	-0.014, 99.985	65.025, 100.035

1	2	3
-65.032, 0.030		65.016, 0.011
-65.017, 0.043	0.0, 0.0	65.005, 0.007
-64.977, 0.061		64.977, 0.030

Figure 5-1. The coordinates (x, y) of the 9 fiducial marks in a Plexiglas plate, determined from three different calibrations. The units are millimeters.

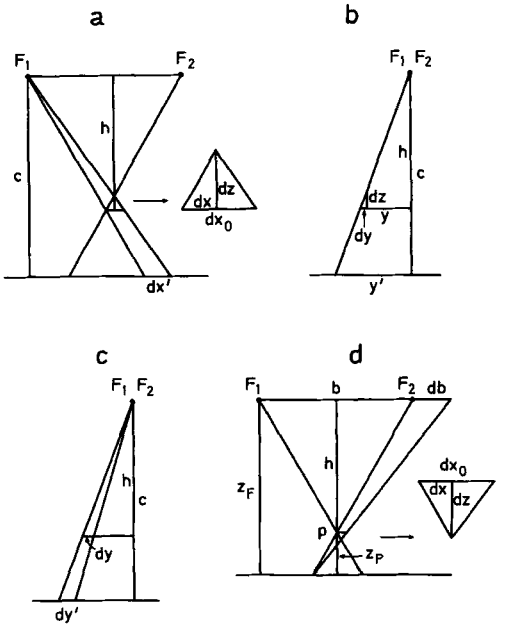

Figure 5-2. Orthogonal projection of rays onto an xz-plane, containing the foci F_1 and F_2 (a, d), and corresponding projections for a yz-plane, perpendicular to the line joining the foci (b, c).

metric normal case. Hallert, however, utilizes a separate coordinate system for each image, but as we have one common coordinate system, his formulas are in some respects not directly applicable to our situation. Especially the influence on model coordinates of errors in the determination of the base, b, is different in the two descriptions.

We shall deduce the influence of errors dx' and dy' in the image coordinates on the model coordinates, using similarity, and study the influence of errors in the determination of the positions of the foci. Our expositions are for Test Cage Model 1, but the principles established could be applied in a discussion of precision errors, obtained when utilizing a test cage of Model 2.

In this section, we study the influence of errors dx' , dy' in the measured object image coordinates on model coordinates. It is sufficient to discuss the error as related to only one of the two image positions. We use h to denote the height from the line joining the foci, downwards in positive direction from the foci towards the film. Figure 5-2a shows an orthogonal projection of rays, defining a model point, into a vertical xz-plane, containing the two foci, F_1 and F_2. From Figure 5-2a, and the enlarged triangle, we have:

$$\frac{dz}{dx_0} = \frac{h}{b} \qquad \frac{dx_0}{dx'} = \frac{h}{c}$$

$(h + dz \approx h)$ which determines the influence of an error dx' on the model z-coordinate

$$dz = \frac{h}{b} dx_0 = \frac{h^2}{bc} dx'$$

Note the influence of the base, b, which is in the denominator.

Turning next to the determination of the error, dx, corresponding to an image error dx', we obtain from the enlarged triangle in Figure 5-2a that $dx \approx dx_0/2$, as the triangle has two nearly equal sides. This is valid for object points centrally placed between foci F_1 and F_2, and our actual objects are not so broad as one-fifth of the base.

Inserting $dx = dx_0/2$ in the second equation above, we obtain:

$$dx = \frac{h}{2c} dx'$$

The model y-coordinate depends both on image x'- and y'-coordinates. With a changed x'-coordinate we also move in y- and z-direction along the line from the foci to the image point. In Figure 5-2b, we see the set-up from the side, where the bottom line is parallel to the y-axis. We temporarily count y- and y'-coordinates from the plumb line from the foci. From similarity follows (Figure 5-2b) that

$$\frac{dy}{dz} = \frac{y'}{c} = \frac{y}{h} \qquad \text{but}$$

$$dz = \frac{h^2}{bc} dx' \qquad \text{so that}$$

$$dy = \frac{yh}{bc} dx'$$

It shall be noted from this formula that the influence of an x'-error varies with the position of the image point. This influence is readily understood from a glance at Figure 5-2b. An error in the z-direction does not influence the y-coordinate for an object point in the vertical plane going through the foci.

The influence of an image error, dy', on the model y-coordinate is shown in Figure 5-2c:

$$\frac{dy}{dy'} = \frac{h}{c} \qquad dy = \frac{h}{c} dy'$$

We summarize, correcting for sign:

$$dx = \frac{h}{2c} dx'$$

$$dy = -\frac{yh}{bc} dx' + \frac{h}{c} dy' \qquad (5:1)$$

$$dz = \frac{h^2}{bc} dx'$$

Passing over from differentials to standard errors, we note that dx' is here composed of the errors from two image coordinates, so for dx' we shall enter $\sqrt{2}$ $s_{x'}$, where $s_{x'}$ is the standard error of one image x'-coordinate. As y' is the mean of the two measurements y'_1 and y'_2, it follows for dy' on the other hand, that:

$$dy' = \frac{dy'_1 + dy'_2}{2}$$

so we shall enter the standard error $1/\sqrt{2} \cdot s_{y'}$ corresponding to dy', where $s_{y'}$ is the standard error of one image y'-coordinate.

Thus, from the law of propagation of errors (see, for example, Hallert, 1967, p. 48):

$$s_x^2 = \left(\frac{h}{2c}\right)^2 2s_{x'}^2$$

$$s_y^2 = \left(\frac{yh}{bc}\right)^2 2s_{x'}^2 + \left(\frac{h}{c}\right)^2 \frac{1}{2} s_{y'}^2 \qquad (5:2)$$

$$s_z^2 = \left(\frac{h^2}{bc}\right)^2 2s_{x'}^2$$

Note that we have a constant base b and film-focus distance c, and study only the variation of object image coordinates.

We have investigated the applicability of these formulas on

1) a determination of the test rod (p. 27) with 22 object points utilizing a test cage of Type 1A, and
2) a determination of the three-dimensional test object with 44 object points utilizing a test cage of Type 1B.

The image has been evaluated with one reconstruction of the interior orientation, but with two determinations of the test object. From this double reading of the object image coordinates we calculate the standard errors $s_{x'}$ and $s_{y'}$, using 2 independent observations from each of n independent samples with the same standard deviations. The formula for the standard error is (Hallert, 1967, p. 27):

$$s_x^2 = \frac{\sum_{i=1}^{n} (x_{i1} - x_{i2})^2}{2 \cdot n} \qquad (5:3)$$

Here 1 and 2 refer to the two determinations of one image point.

Evaluation of the test rod (Paragraph 1, above). We used here a roentgenogram, industrial film, with the test object 15 mm above the film and in a Test Cage 1A. The distance between the foci b = 480 mm, the film-focus distance c = 1120 mm, and the height h = 1105 mm. From the two images of 22 tantalum pins we get n = 2 x 22 image points. From the double reading we determine $s_{x'}$ = 11.0 μm and $s_{y'}$ = 4.6 μm. The pins are orientated in x-direction, and we focus on the pointed end of the pin, so we expect less precision in x-direction than in y-direction.

From the photogrammetrically determined model coordinates, a determination which is done twice for

Table 7. The standard error (SE) from photogrammetrically determined model coordinates and deduced standard errors from image coordinates using Formula 5:2. Unit: μm

SE	s_x	s_y	s_z
Model coordinates	*8.5*	*3.7*	*30.7*
Calculated (Formula 5:2)	*7.7*	*3.2*	*35.2*

Table 8. The standard error (SE) of one image coordinate (x'/y') for the two planes of the 3-D test object in a Cage Model 1B, each containing 22 object points. Unit: μm

SE	$s_{x'}$	$s_{y'}$
Lower plane	*26.1*	*30.1*
Upper plane	*23.9*	*28.1*

every object point, we now compute s_x, s_y and s_z for n = 22 points. For comparison we calculate the values of the model standard errors from the formulas (5:2).

In Table 7, actual model standard errors are compared to these deduced standard errors.

Comment: The value for s_y, computed from the image coordinates, has been calculated using only the second term in the Formula 5:2b. The maximum value of y for the test rod indicators is 100 mm, so the coefficient of $s^2_{x'}$ is maximally $(100/480)^2 \cdot 2 \cdot 2 = 0.17$ times the coefficient of $s^2_{y'}$. But the quotient between $s^2_{x'}$ and $s^2_{y'}$ is 5.7, using the earlier given $s_{x'}$ and $s_{y'}$. The influence of the errors in x'-determinations will thus be as large as the influence of the errors in the y'-determination for the end-points of the rod. The calculated value of $s_{y'}$ for an end-point is 4.5 μm. The fact that different points of the test rod are determined with different precision due to their different distances from the midpoint of the cage should be regarded in a more precise determination of the errors. However, as the errors are larger in the periphery than in the central parts of the test cage, and we use the central part in actual clinical length determinations, we shall be more apt to overestimate than underestimate the irregular errors, when including all points of the rod.

Evaluation of the three-dimensional test object (Paragraph 2, above). We utilize a test cage of Model 1B, and as usual with this type of cage, we roentgenograph the object on a film between intensifying screens. As we have two different heights of the indicators, we evaluate each plane separately which contains 22 object points. From these we get two groups each having n = 2 x 22 double-measured image points. We obtain the values for the standard errors of image coordinates (Table 8).

The lower plane of object points is at a height of h = 980 mm from the foci, and the upper plane is at a height of h = 900 mm. The distance between the foci is b = 660 mm, and the film-focus distance is c = 1210 mm. As in the earlier case, we exclude the errors in the x'-coordinate when calculating the standard error of the model y-coordinate from

Table 9. The standard error (SE) of one object coordinate (x/y/z) for the two planes of the 3-D test object in a Cage Model 1B from photogrammetrically determined model coordinates and deduced standard errors from image coordinates using Formula 5:2. Unit: μm

SE	Lower plane			Upper plane		
	s_x	s_y	s_z	s_x	s_y	s_z
Model coordinates	*14.2*	*17.0*	*41.5*	*13.2*	*16.0*	*36.2*
Calculated (5:2)	*14.9*	*17.2*	*44.4*	*12.6*	*14.8*	*34.2*

standard errors of the image coordinates. This might be more justified in this case, as the coefficient of $s^2_{x'}$ is maximally $(100/660)^2 \cdot 2 \cdot 2 = 0.09$ times the coefficient of $s^2_{y'}$ and $s_{x'}$ itself is smaller than $s_{y'}$ (Tables 8 and 9).

Irregular errors in the determination of positions of the foci and their influence on model coordinates

In Chapter 3 we have discussed how systematic errors can arise in the determination of the foci coordinates due to errors in the calibration of the plate with the control points. We will now discuss the irregular errors in the determination of the foci, and how these errors influence the model coordinates. Positional errors can be viewed as a common translation error of the two foci and a relative displacement between the two foci. We study a common translation of the two foci in the x-, y- and z-directions, and a variation in the distance b between the foci.

A common translation of the two foci: A model point, P, is obtained as the intersection of the two lines between the foci and the images $\bar{r}_{01}$ and $\bar{r}_{02}$ of the point in the plane of the fiducial marks:

$$\bar{r}_{P1} = \bar{r}_{01} + t_1 (\bar{r}_{F1} - \bar{r}_{01})$$

$$\bar{r}_{P2} = \bar{r}_{02} + t_2 (\bar{r}_{F2} - \bar{r}_{02})$$

For the case $z_{F1} = z_{F2} = z_F$ we have, as the plane of the fiducial marks is the plane z = 0:

$$z_{P1} = t_1 z_{F1} = z_{P2} = t_2 z_{F2}$$

$$t_1 = t_2 = \frac{z_P}{z_F}$$

If we translate the foci an equal amount $\Delta\bar{F}_1 = \Delta\bar{F}_2 = \Delta\bar{F}$, the new model coordinates are obtained from:

$$\bar{r}_{P1,tr} = \bar{r}_{01} + t_1 (\bar{r}_{F1} + \Delta\bar{F} - \bar{r}_{01})$$

$$\bar{r}_{P2,tr} = \bar{r}_{02} + t_2 (\bar{r}_{F2} + \Delta\bar{F} - \bar{r}_{02})$$

and we see that these two lines intersect, and that the model point $\bar{r}_{P,tr}$ is:

$$\bar{r}_{P1,tr} = \bar{r}_P + \Delta\bar{r}_P = \bar{r}_P + \frac{z_P}{z_F}\Delta\bar{F}$$

Thus, if the foci are translated an amount $\Delta\bar{F}$, this leads to a translation $\Delta\bar{r}_P$ of a model point, P:

$$\Delta\bar{r}_P = \frac{z_P}{z_F}\Delta\bar{F} \qquad (5:4)$$

A common translation of the foci in the direction of one coordinate axis influences only the model coordinate along this axis. From the formula, we see that a translational error in foci coordinates will lead to a constant error for model coordinates in an object plane parallel to the plane of fiducial marks, i.e. in a plane z_P = constant. It is important that this be noted. Only when we compare points in planes at different heights will the errors discussed here have any influence.

For Test Cage Models 1A and 1B, respectively, we have obtained the standard errors of the common translations of the foci, in x-, y- and z-directions, from ten double determinations of the positions of the foci (Table 10).

Comment: The fact that the error in the z-direction is smaller for a test cage of Type 1B than for a test cage of Type 1A, is explained by the fact that the control points are more widely spaced, both in x- and y-direction, in the first-mentioned cage.

The errors in the determination of the foci lead to model errors between planes z = constant in an object, and for two points with a difference in height of Δh, we denote the errors dx_h, dy_h and dz_h. To give an example of the magnitude of these errors, we consider the three-dimensional test object, where the distance, Δh, between the two planes of indicators is 80 mm. The foci errors are assumed to

Table 10. The standard errors (SE) of the common translations of the foci in x-, y- and z-directions from ten double determinations of the positions of the foci. Unit: μm

SE	s_{Fx}	s_{Fy}	s_{Fz}
Test Cage 1A	***116***	***22***	***620***
Test Cage 1B	***98***	***49***	***218***

Table 11. Model coordinate errors (d) for two points with a difference in height of 80 mm in the three-dimensional test object, caused by errors in determination of the foci. Unit: μm

	dx_h	dy_h	dz_h
Test Cage 1A	**8**	**1.6**	**44**
Test Cage 1B	**8**	**4**	**17**

be the standard errors above. The heights, z_F, of the foci in the examples of the preceding section were for Test Cages 1A and 1B, equal to 1120 mm and 1000 mm, respectively, and utilizing these values, we obtain the model errors (Table 11).

An error in the distance b between the foci: We shall demonstrate the influence on model coordinates of an error, db, in the base, b.

Figure 5-2d depicts the two foci and a model point, P. From similarity between the triangle with base, b, and the enlarged triangle, (db<<b), we get:

$$\frac{dz}{dx_0} = \frac{h}{b}$$

and again from similarity, ($dz << z_P$):

$$\frac{dx_0}{db} = \frac{z_P}{z_F}$$

Elimination between these equations gives:

$$dz = \frac{hz_P}{bz_F}db$$

Consequently, as

$$dy = \frac{y}{h}dz$$

(Figure 5-2b), we get:

$$dy = \frac{yz_P}{bz_F}db$$

and in analogy with the earlier discussion, that $dx \approx dx_0/2$:

$$dx = \frac{1}{2}\frac{z_P}{z_F} db$$

We summarize the influence of an error db in the base, b, correcting for sign:

$$dx = \frac{1}{2}\frac{z_P}{z_F} db$$

$$dy = \frac{y}{b}\frac{z_P}{z_F} db \qquad (5:5)$$

$$dz = -\frac{h}{b}\frac{z_P}{z_F} db$$

The mean translation, dx_F, in the x-direction is $0.5 \cdot (dx_{F1} + dx_{F2})$, and the error, db, in the base is $db = dx_{F1} - dx_{F2}$. Thus $s_b = 2s_{Fx}$, and from the earlier given values of s_{Fx}, we deduce $s_b = 232$ µm and $s_b = 196$ µm for Test Cages 1A and 1B, respectively.

To give an example, we again examine the errors of model coordinates of the upper plane of the three-dimensional test object. We observe that the error in the y-direction now depends on the actual y-coordinate of the object point, and choose the uttermost indicator (y = 100 mm) for the example. The errors are denoted as dx_{hb}, dy_{hb} and dz_{hb}, and are errors for a point relative to another point with a difference in height of $\Delta h = 80$ mm.

We then have for Test Cages 1A and 1B with z_F = 1120 mm and 1000 mm, respectively, and base b = 480 mm and 660 mm, respectively (values according to Table 12).

In Chapter 3, we found that the determination of the position in x- and y-directions of the plate of control points was done with a precision of (32, 8) µm and (32, 44) µm for a test cage of Models 1A and 1B, respectively. Thus, for the test object, the systematic errors in x- and y-directions between the two planes of indicators, due to an error in the calibration of the magnitude of the standard error, will be (18, 5) µm and (17, 23) µm, for Test Cages 1A and 1B, respectively (Formula 3:5). These errors are thus larger than the discussed irregular errors from determinations of the foci.

Table 12. Model coordinate errors (d) for two points with a difference in height of 80 mm in the three-dimensional test object, caused by errors in determination of the base. Unit: µm

	dx_{hb}	dy_{hb}	dz_{hb}
Test Cage 1A	**8**	**3.5**	**36**
Test Cage 1B	**8**	**2.4**	**22**

The roentgen stereophotogrammetric method used for measuring length

The precision in determining the y-coordinates of an object is high when using a test cage of Model 1A and industrial film. We showed (p. 25) that the precision, expressed as the standard error, when using a well-defined object, is 3.7 µm for the y-coordinate. Thus, when we have an object where lengths to be determined are along the y-direction, we can maximally expect the lengths to be determined with an accuracy of $\sqrt{2} \cdot 3.7$ µm = 5.2 µm.

The test rod: We have constructed a test object in the form of a 200 mm long rod with 11 pointed tantalum pins on each side of the rod, one row pointing to the left and the other row pointing to the right. The points of the tantalum pins in each row lie on the line, and the distance between two pins is 20 mm.

We use this test object to ascertain the accuracy by which lengths are determined using the roentgen photogrammetric procedure. The test rod is to function as a standard, and must, then, be calibrated with high accuracy. To reach what might be a higher accuracy than in our Autograph A8, we calibrated the test rod twice in a Zeiss Stecometer, a high-precision photogrammetric instrument (mean square error of coordinate measurement = 2 µm), and once in the Wild Autograph. The values used are the means of five settings. The standard deviation for one setting was, in the mean over all the 22 indicators less than 5 µm for both instruments.

We utilize the first calibration in the stecometer as the standard for the roentgenographic measurements.

To compare the values of length obtained from a roentgenogram with the standard, different procedures can be used. We have a computer program GROWTH, that computes and compares the lengths between all combinations of points in a model for two times. Having 11 measurement points in the test rod, we have 55 different combinations of distances, and the mean of these distances is 80 mm. As all combinations of distances and the corresponding differences are computed by the program, the squared sum of the differences is easy

Table 13. The root mean square value (RMSV) and the standard error (s_0) when determining the length of a two sided test rod compared with the values for length obtained with the Stecometer. Unit: µm

	Side 1		Side 2	
	RMSV	s_0	RMSV	s_0
First film	7.5	*4.4*	14.9	*4.4*
Second film	12.8	*9.0*	12.8	*4.6*

Table 14. The root mean square value (RMSV) and the standard error (s_0) when comparing the length of a two sided test rod measured with the Stecometer with the values for length obtained in a second evaluation and in the Autograph. Unit: µm

Evaluation	Side 1		Side 2	
	RMSV	s_0	RMSV	s_0
Autograph	5.4	*4.1*	5.2	*3.9*
Second Stecometer	5.8	*4.2*	6.5	*3.6*

to obtain. We compute the root mean square value (RMSV) of these differences as:

$$RMSV = \sqrt{\frac{\sum_{i=1}^{55} \left(l_{ip} - l_{is}\right)^2}{55}}$$

where l_{ip} is the actual measured length, and l_{is} is the standard length from the calibration.

A systematic error proportional to the distance measured, will show up in the determinations of lengths, if the measurement is done in a test cage of Plexiglas not having the temperature under which it was calibrated. The coefficient of thermal expansion for Plexiglas is, as earlier stated, $75 \cdot 10^{-6}$/°C. This means an expansion of 15 µm/°C for the distance (200 mm) between the proximal and distal rows of fiducial marks in Test Cage Model 1A. The Plexiglas test cage is calibrated for 23.5°C. If the actual measurement of the test rod is carried out at a temperature 1°C higher, the computed values for a test length of 200 mm will be 15 µm shorter, as the perspective transformation will shorten a distance of 200 mm in the image by this amount when transforming back to the given values of the fiducial marks. Note that the test rod, made of quartz glass, has a coefficient of thermal expansion of $3.2 \cdot 10^{-6}$ /°C, corresponding to a change in length of 0.64 µm/°C for a length of 200 mm, so its own thermal expansion can be neglected.

Irregular errors in measuring the fiducial marks on the film can be shown to contribute with an error of about 5 µm to the distance between the proximal and distal rows of fiducial marks.

Hallert (1967, p. 54) describes the calibration of a gauge rod. The discrepancies between measured values and given values are assumed to depend on irregular errors and two systematic errors. The systematic errors are: 1) a translation of the origin of the rod and 2) a scale error, proportional to the distance of the actual indicator from the origin. The scale error is, in our case, proportional to a faulty temperature when exposing the roentgenogram, among other things. After adjustment for the two systematic errors, the standard error of the procedure, now only containing observational errors, can be calculated. The two corrections are determined minimizing the squares of discrepancies between measured and given values, and the standard error s_0 is computed from the remaining errors vi after the adjustment:

$$s_0 = \sqrt{\frac{\sum_{i=1}^{n} v_i^2}{n - 2}}$$

In our case, n = 11. The second term in the denominator n-2 comes from the two parameters.

In a test, we exposed the rod twice on industrial film, utilizing a Test Cage 1A and at the level z = 15 mm. The test rod was parallel to the y-axis of the cage. We obtained values for the RMSV and the standard error s_0, for the two sides of the rod, when the values of length from the images were compared with the first measurement in the Stecometer (Table 13).

This can be compared to the values obtained from comparing the first evaluation in the Stecometer with the second evaluation in this instrument and with the evaluation in the Autograph (Table 14).

The root mean square value RMSV is obtained from differences in lengths, and the standard error s_0 is the error in the determination of the y-coordinate of one point. Were it not for systematic errors, we thus should in principle have $RMSV = \sqrt{2} \cdot s_0$.

It is obvious that our roentgen photogrammetric method is successful in determining lengths, as we have practically the same accuracy s_0 for one setting on the roentgen image as we obtain from the mean of five direct measurements on the rod. Temperature effects ought to be better controlled, and this can be achieved by using glass instead of Plexiglas in the construction of the test cage.

Determination of accuracy and precision in the reconstruction of a three-dimensional test object

The three-dimensional test object, made from quartz glass and with 0.4 mm steel balls as indicators, which was described in Chapter 3 (Figure 3-1), has been used to ascertain the accuracy and precision in determining the three-dimensional positions of ball indicators. The size of the testing area of the object is 200 x 90 x 80 mm, and the 44 indicators are spaced at equal distances on thee four long sides of the object. We have roentgenographed the object, utilizing both a test cage of Model 1B, and a test cage of Model 2.

The tests correspond to actual clinical investigations, where we for truly three-dimensional examinations utilize one of these test cages, 1B or 2, the choice of which depends on the size of the object. The films, cassettes, screens and grids are also the same as used in clinical investigations.

The test object is calibrated from the mean of two determinations in a test cage of Model 1A, as was discussed in Chapter 3. The z-coordinates of the indicators are separately determined from two roentgenograms of the test object, viewed from the side.

After having determined model coordinates of the test object, we compare the values obtained with the standard, calibrated in the manner described. The comparison is performed by finding the best correspondence between the two clusters of points, treated as rigid bodies, and when this correspondence has been found, the mean of the distances between the standard points and the model point can be given. We utilize here a part of the computer programme KINEMA, described in Chapter 7. The root mean square value of the distances between standard and model points is obtained from the same formula (7:1), which in Chapter 7 expresses the mean error of rigid-body fitting. The two usages, here and in Chapter 7, are identical.

Test Cage Model 1B: The film is in a cassette, size 40 x 70 cm, supplied with universal screens (Kruppa). For two determinations of the test object, we obtained the root mean square value (RMSV) of distances between standard and model coordinates to 98 and 94 μm, respectively. This radial error is an expression of the accuracy of the method. When we reevaluated the two images, the comparison between the first and second determinations gave a RMSV of distances of 78 and 73 μm, respectively, which values are expressions of the precision in the method.

Table 15. Precision measured as the root mean square values when using Test Cage Model 2 and industrial film or film between high definition screens and a grid. Unit: μm

Comparison with	No grid		Grid	
Standard	35	30	48	47
Preceding evaluation	18	20	43	38

Note: By accuracy is meant the closeness of measurements to the true value, and expressions for this are obtained when comparing the actual measurements with a standard. By precision is meant how repeated observations conform to one another (see, for example, Kendall-Buckland, 1957).

The irregular errors of one point are $1/\sqrt{2}$ of the precision RMSV, as the latter is composed of errors from the determinations of two points, the coordinates of which both show the same dispersion. Thus, the irregular error for one point is, in the two determinations, 55 and 52 μm, respectively. This is due to errors in the determination of object image coordinates and the elements of interior orientation. The radial errors for points due to image irregular errors were, for points in the lower and upper plane of the test object, using the earlier determined standard errors (p. 25), 47 and 42 μm, respectively. Errors in the elements of the interior orientation account for thee remaining part up to the total errors of slightly more than 50 μm.

Comment 1: Comparing the two evaluations of the three-dimensional object, which we earlier utilized for determining the standard errors of model coordinates, with the method of this section, we obtain 42 μm as the mean radial error for one point. The earlier method had given 47 μm and 42 μm for the radial errors, as has just been mentioned.

Comment 2: The irregular error in determining a point was shown to be about 50 μm. The lack of accuracy, which was expressed as a radial error of the order of 100 μm, depends partly on this irregular error, but it further depends on 1) bending of the film, 2) faulty calibration of the test cage and 3) only seeming errors due to faulty calibration of the standard. We assume that bending of the film is the most important source of errors in this connection.

Test Cage Model 2: We have made tests utilizing 1) industrial film and 2) film between high-definition screens (Rubin, Siemens) and a grid (90 lines/inch). The results of two evaluations of each case, where we have also reevaluated all four films, are the root mean square value of the distances between points (Table 15).

The precision for one determination of a point is $1/\sqrt{2}$ of the values given in the second line above, as we compare two separate evaluations. We thus have an irregular error in the determination of the space coordinate of a point of about 14 μm when exposing on industrial film, and the irregular error is about 30 μm when using a grid. The lack of accuracy must, besides irregular errors, be related to calibration errors of the test cage or the test object. The rays strike the films at approximately right angles, so bending of the films is of lesser importance here than when utilizing a test cage of Model 1B. We also have smaller film sizes (24 x 30 cm).

6. Kinematics of rigid bodies

Terminology and introduction

Mechanics is the study of the motion of material bodies. The description of motion in mathematical terms is called *kinematics* and is independent of the cause of the motion. The study of motion due to various causes is called *kinetics* or *dynamics*. An important special aspect of dynamics is *statics*, or the lack of motion due to various causes.

A *rigid body* is defined as a system of mass-points subject to the constraints that the distances between all pairs of points remain constant throughout the motion (Modified from Fox 1967 and Goldstein 1950).

The rigid body is a mathematical model of the behaviour of some physical bodies. The advantage of the model lies in the fact, that the motion of a rigid body can be described using only a few parameters, and correspondingly, the motion can be determined by only a few measurements. Non-rigid bodies are called deformable. To determine and describe the motion of a deformable body is usually, in practical circumstances, an exceedingly complex task.

The rigid-body model: Segments of continuous bone can be described as rigid bodies in a large number of situations. The elastic deformation of bone under normal stresses occurring *in vivo* is slight. Note that the properties "rigid" and "deformable" do not mutually exclude each other, but depend on the circumstances under which the bone is studied. Even the very same piece of bone, that was once a part of a link mechanism of the skeleton, and was there treated as a rigid body, can be removed and tested for its elastic behaviour.

We cited a definition of mechanics, and its subdivisions kinematics, statics, and dynamics at the beginning of this chapter. More informally we can say that kinematics covers the description of motion (including the description of deformation of non-rigid bodies), that statics introduces the concept of force and describes the equilibrium between forces, and that dynamics is the general theory connecting forces, masses, and motions. In our study we limit ourselves to the study of kinematics. Though incomplete from a general point of view, results won under these limitations may be of great significance, both theoretically and from a practical standpoint.

The number of degrees of freedom of a rigid body

By the number of degrees of freedom is meant the (least) number of parameters which are needed to define the position of a rigid body in space. The number of degrees of freedom is six. This can be established in several ways, and we account for four of these ways here:

1. The position in space of three noncollinear points in the body obviously determines the position of the whole rigid body. (If the three points were collinear, the body could rotate about the axis joining these points.) The three distances between the points are not dependent on the actual configuration, so the number of degrees of freedom is 3 x 3 (three points and in three-dimensional space) minus 3 (the invariant distances), equalling 6 (six degrees of freedom).

2. If one point of the rigid body is fixed to its final position, utilizing three degrees of freedom, a second point might move on a sphere centered at the first point. The fixation on the sphere of the second point (latitude and longitude) utilizes two degrees of freedom, and the rigid body might still rotate about the axis joining these two points. The angle, a third point in the body makes with a fixed direction from the rotation axis, determines the final position of the body, which thus needed 3 + 2 + 1 = 6 parameters for its specification.

(3 + 4). In the ensuing mathematical exposition, we shall use two main modes of description of the motion of a rigid body. In the first mode, we describe the rigid-body motion as a transformation of points in space, assigning new coordinates $\bar{r}$ to a point $\bar{r}_0$ (0 = reference time) by:

$$\bar{r} = M\bar{r}_0 + \bar{d} \qquad (6 : 1)$$

where M is a 3 x 3 rotation matrix and $\bar{d}$ is a translation vector, both of which will be discussed in detail later on. In the second mode, we describe the motion as a screw motion, that is a rotation about a certain axis (the screw axis) followed by a translation along this axis.

3. In the transformation of all points $\bar{r}_0$ in the rigid body by

$$\bar{r} = M\bar{r}_0 + \bar{d}$$

the translation $\bar{d}$ is obviously independent of the rotation M, as we can add an arbitrary translation to any given rotation. Thus we have three translatory degrees of freedom. That the matrix M depends on only three parameters (= rotation angles) was proved by Euler, and is here discussed elsewhere. The matrix M is thus determined by three rotational degrees of freedom, and we have, as in paragraph 2 above, three translational and three rotational degrees of freedom.

4. The screw axis, being a line, is defined by a point on the line and the direction of the line. The point on the line can with advantage be taken as the intersection of the screw axis with one of the coordinate planes, necessitating the two-dimensional coordinates in this plane. The direction of the line is specified by a vector along the screw axis, but as the length of the vector can be chosen equal to 1, the vector has only two independent components. With a given rotation angle about the screw axis, and given translation along it, the position of the rigid body will be completely determined, utilizing totally 2 + 2 + 1 + 1 = 6 parameters.

The displacement of a rigid body

The rigid body has two fundamental modes (forms) of displacement: translation and rotation. Translation is a displacement such that every point of the body has the very same movement. Rotation is a displacement such that points on a line (the rotation axis) remain unchanged, and points outside this line move in proportion to their distances from the line.

Euler (1776) proved that the general displacement of a rigid body with one fixed point is a rotation about an axis through this point. A corollary to this theorem is that the general displacement of a rigid body is the sum of the translation of a base point and a rotation about this base point. This is obvious since the displacement of one point is, by definition, a translation, and if we move one arbitrarily chosen point from its original to its final position, this point (called the base point) can for our further exposition be regarded as the fixed point under discussion in Euler's theorem.

Euler also showed (1776) that the general rigid-body displacement is represented by a transformation:

$$\bar{r} = M\bar{r}_0 + \bar{d}$$

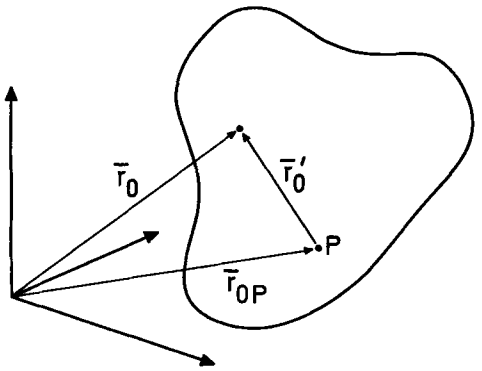

Figure 6-1. Position vector r'_0 in relation to a base point P.

which to every position vector $\bar{r}_0$ in the rigid body assigns its value $\bar{r}$ after the motion. This is our notation. In Chapter 1 we have reproduced Euler's notations in the original work. M is the rotation matrix, whose nine coefficients are constants for a certain motion, and $\bar{d}$ is the displacement vector. The vector $\bar{d}$ is the translation of the point in the rigid body coincident with the origin of the coordinate system before the displacement. This point is thus the base point. For an exposition of matrix notations, consult Chapter 8.

If the displacement is not a pure translation, it is obvious that the translation in general is different for different choices of base point. Of utmost importance, however, is the fact that the rotation is independent of the base point.

An expression for the translation $\bar{d}_P$ of a second base point, P, is obtained if we substitute $\bar{r}_0$ by $\bar{r}_{0P} + \bar{r}'_0$, where $\bar{r}'_0$ is the vector relative to P for a point in the body (Figure 6-1). We have

$$\bar{r} = M(\bar{r}_{0P} + \bar{r}'_0) + \bar{d}$$

$$\bar{r} = M\bar{r}'_0 + \bar{d} + M\bar{r}_{0P}$$

and with $\bar{d}' = \bar{d} + M\bar{r}_{0P}$

$$\bar{r} = M\bar{r}'_0 + \bar{d}'$$

This proves that the translation $\bar{d}_P = \bar{r}_P - \bar{r}_{0P}$, the change of position of a point P is

$$\bar{d}_P = \bar{d} + (M - I)\bar{r}_{0P} \qquad (6 : 2)$$

(I = the identity matrix), but it also proves that the rotation matrix is independent of the choice of base point. (The expression for the translation $\bar{d}_P$ could

of course, have been obtained through direct substitution of $\bar{r}_0 = \bar{r}_{0P}$ in the main equation 6:1).

Returning to the theorem of Euler and the rotation axis, we can ask if there is any relation between the direction of the translation and the direction of the rotation axis. In general, the answer is no. A wise choice of the base point can be made, however, so that the translation of the base point is along the rotation axis. This fact is called Chasles' theorem (1830). The displacement, viewed in this way, can obviously be interpreted as a screw displacement, but the actual displacement may, of course, not have taken place as stepwise screw movements.

The screw axis is the axis of rotation most closely approximating the pure rotation axis, as the translation of the points on the screw axis is smallest for all points in space moving with the rigid body. The translation for a point is the sum of the screw translation and a movement due to the rotation, and the latter movement is proportional to the distance of the point from the screw axis. Note that the screw axis, may not pass through the rigid body, although this is the case in Figure 7-1, which depicts screw motion.

In summary, we give preference to two modes of description of rigid-body motion: 1) A description utilizing the rotation matrix M and a translation vector, and 2) A description in terms of screw displacement. In certain experimental settings either mode of description might be of advantage. In the next section we shall show that various interpretations of the rotation matrix M exist, and we have already discussed the dependence of the translation on the choice of base point. The description in terms of screw displacement is, however, unique.

The presentation of the rotation matrix as a function of three rotation (Eulerian) angles

A Cartesian coordinate system (x, y, z) is fixed in space. A rigid body is moving with another Cartesian coordinate system (X, Y, Z) fixed to the body. In the reference configuration, the directions of the axes of the moving coordinate system coincide with the directions of the axes of the fixed coordinate system. We intend to describe the motion of the rigid body as a motion of the body-fixed coordinate system relative to the space-fixed system.

The description of the motion is mathematically achieved by determining a matrix M and a vector $\bar{d}$.

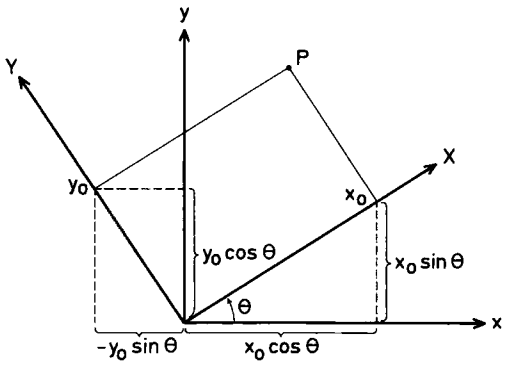

Figure 6-2. A rotation of the body-fixed coordinate system about the z = Z-axis through an angle θ.

This matrix M and vector $\bar{d}$ transform a point $\bar{r}_0$ in the body from its reference position $\bar{r}_0$ to its position $\bar{r}$ after a displacement:

$$\bar{r} = M\bar{r}_0 + \bar{d}$$

Euler (1776) proved that the nine components of the rotation matrix M could be expressed as functions of three parameters. We shall show how these parameters can be physically interpreted as rotation angles about coordinate axes, fixed in space or in the body.

In this section, we shall discuss pure rotations, and find the decomposition of the rotation matrix M as a product matrix of rotations about the three space-fixed or the three body-fixed coordinate axes.

The single rotation about one coordinate axis. Consider a single rotation through an angle θ (in the right-handed sense) about the positive z = Z-axis (Figure 6-2). The coordinates for a vector

$$OP = \bar{r}_0 = (x_0, y_0, z_0)$$

fixed in the body, are after rotation of the body-fixed coordinate system through an angle θ:

$$x_\theta = x_0\cos\theta - y_0\sin\theta$$
$$y_\theta = x_0\sin\theta + y_0\cos\theta$$
$$z_\theta = z_0$$

where x_θ, y_θ and z_θ are the coordinates of the vector in the space-fixed system. This follows from the constructions in Figure 6-2. The coordinates of the vector in the body-fixed system are according to the definition not changed by this transformation.

Using matrix notations, the discussed rotation through an angle θ about the z = Z-axis is written:

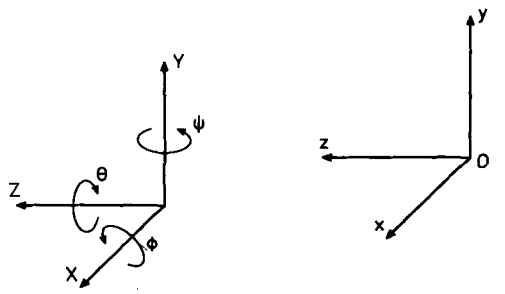

Figure 6-3. The rotations through angles ϕ, ψ and θ about the body-fixed X-, Y- and Z-axes.

$$\begin{bmatrix} x_\theta \\ y_\theta \\ z_\theta \end{bmatrix} = \begin{bmatrix} \cos\theta & -\sin\theta & 0 \\ \sin\theta & \cos\theta & 0 \\ 0 & 0 & 1 \end{bmatrix} \begin{bmatrix} x_0 \\ y_0 \\ z_0 \end{bmatrix} \qquad (6:3a)$$

$$\bar{r}_\theta = M_\theta \bar{r}_0$$

In the same way we define rotations through angles ϕ and ψ in the right-handed sense about the positive x = X and y = Y-axes, and find their representation by the matrices M_ϕ and M_ψ (Eq. 6:3b and 6:3c):

$$M_\phi = \begin{bmatrix} 1 & 0 & 0 \\ 0 & \cos\phi & -\sin\phi \\ 0 & \sin\phi & \cos\phi \end{bmatrix} \quad M_\psi = \begin{bmatrix} \cos\psi & 0 & \sin\psi \\ 0 & 1 & 0 \\ -\sin\psi & 0 & \cos\psi \end{bmatrix}$$

Composite rotations about space-fixed axes. It is evident that if rotation first takes place about the x-axis, then about the y-axis, and at last about the z-axis, the matrix M for the composite rotation is:

$$M = M_\theta M_\psi M_\phi \qquad (6:4)$$

as the directions x, y and z in space are unchanged. This is the complete formula for composite rotations about space-fixed axes.

Composite rotations about body-fixed axes. If rotation first occurs about the x = X-axis, and then about the body-fixed Y-axis, the direction in space of the Y-axis has been changed by the first rotation, and we can not directly apply the above formula. As it is of interest to follow the rotations about body-fixed axes, we shall show how the rotation matrix M = $M_{\phi\psi\theta}$ for composite rotations about body-fixed axes can be expressed using the three matrices deduced above.

The three successive rotations about body-fixed axes are (Figure 6-3):

1) An initial rotation ϕ about the x = X-axis
2) A secondary rotation ψ about the Y-axis
3) A tertiary rotation θ about the Z-axis.

Theorem: The product matrix M = $M_{\phi\psi\theta}$ for rotations ϕ, ψ and θ, in that order, about three orthogonal body-fixed axes X, Y and Z, is:

$$M_{\phi\psi\theta} = M_\phi M_\psi M_\theta \qquad (6:5)$$

where M_ϕ, M_ψ and M_θ are the rotation matrices for rotations ϕ, ψ and θ about the space-fixed x-, y- and z-axes.

Note that the order among the matrices is reversed when turning from space-fixed axes to body-fixed.

Proof: We give the proof for three general matrices A, B, and C, for each of which there is an inverse, A^{-1}, B^{-1}, and C^{-1}, respectively, and which are defined in the original (reference) coordinate system.

The matrix A transforms the original configuration with position vectors $\bar{x}$ to a new configuration with position vectors $\bar{x}' = A\bar{x}$.

The matrix B is to operate upon these transformed vectors $\bar{x}'$, but its definition is given in the original coordinate system, which is now transformed.

Let B operate upon an arbitrary vector $\bar{x}$ in the original coordinate system, giving a vector $\bar{y}$, with $\bar{y} = B\bar{x}$. The transformation of these vectors with A yields $\bar{y}' = A\bar{y}$, $\bar{x}' = A\bar{x}$, and, thus, $\bar{y} = A^{-1}\bar{y}'$, $\bar{x} = A^{-1}\bar{x}'$. If we put this in the equation for transformation by B in the original system, we get:

$$A^{-1}\bar{y}' = BA^{-1}\bar{x}'$$
$$\bar{y}' = ABA^{-1}\bar{x}'$$

and find the expression $B' = ABA^{-1}$ for B in the coordinate system transformed by A. Returning to the original vector $\bar{x}$, we put $\bar{x}' = A\bar{x}$ in the last equation:

$$\bar{y}' = ABA^{-1}A\bar{x}$$
$$\bar{y}' = AB\bar{x}$$

where $\bar{y}'$ gives the coordinates in the original system for the vector $\bar{x}$, first transformed by A and then by B. The third matrix C, also defined in the original system, has the expression $ABC(AB)^{-1}$, when operating on vectors already transformed twice, and the complete transformation is thus : $ABC(AB)^{-1}AB = ABC$.

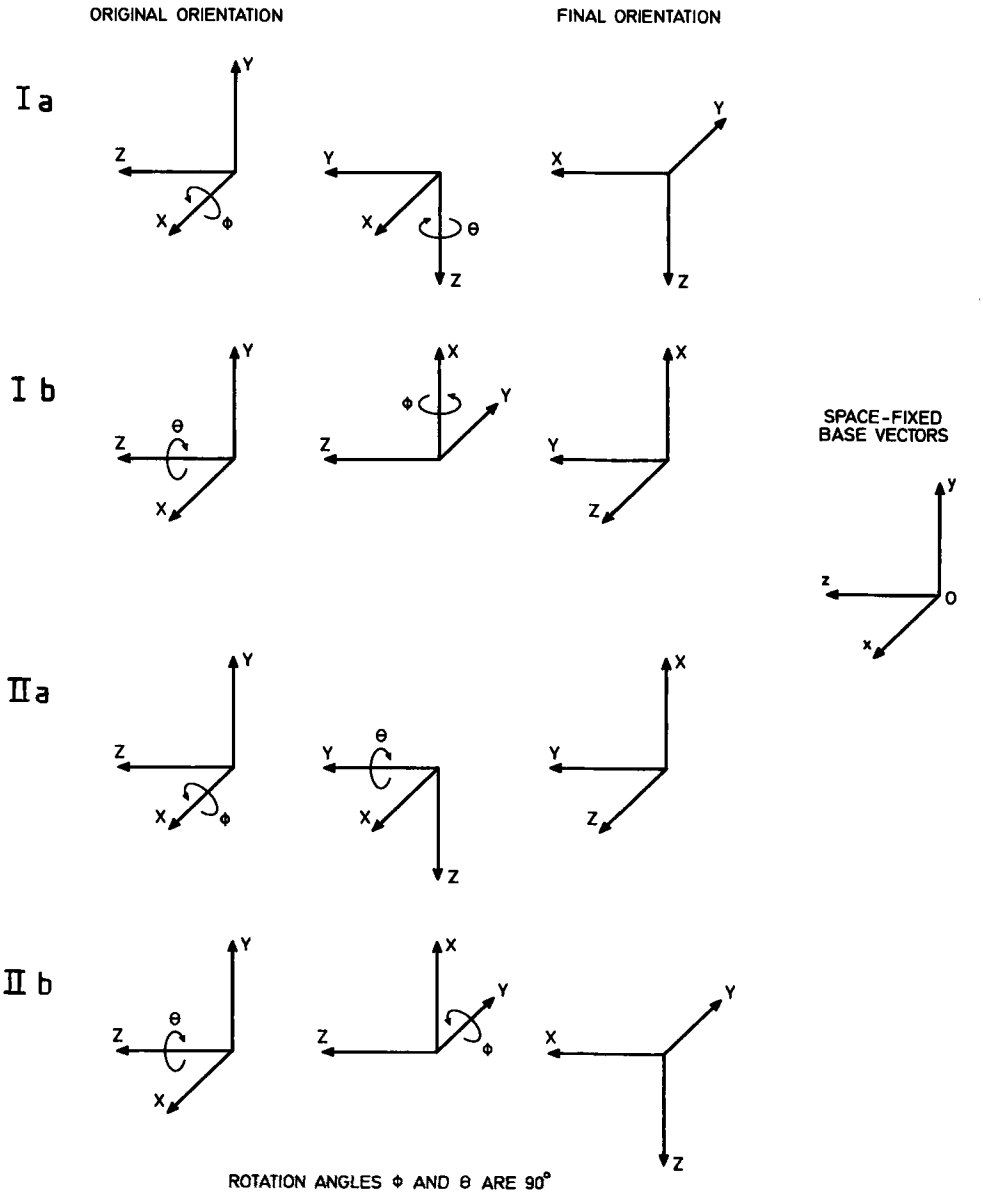

Figure 6-4. Rotations through 90° about body-fixed axes (I) and space-fixed axes (II). See the text.

Putting $A = M_\phi$, $B = M_\psi$ and $C = M_\theta$, which is allowed, as the rotation matrices obviously have inverses, we have proved our statement.

An illustrative example. The rotation of an object can be interpreted as having been achieved by successive rotations about body-fixed or space-fixed axes. By giving an example, we shall illustrate the following three propositions, namely:

1) Rotating an object through the same angles, in the first case about body-fixed axes and in the second case, about space-fixed axes, leads to different final orientations of the object.

2) Rotating an object through certain angles about body-fixed axes is equivalent to rotating the object through the same angles about space-fixed axes, but in the reverse order. *Comment:* This is obvious since the matrix $M_{\phi\psi\theta}$ for rotations ϕ, ψ and θ, in that order, about body-fixed axes has been proved to be

equal to $M_\phi\ M_\psi\ M_\theta$, which is the matrix for rotations about space-fixed axes through the same angles θ, ψ and ϕ, but in the order z, y and x. The reader is reminded that matrix multiplication is not commutative.

3) The order in which the rotations of an object about different axes are to be performed must be specified. The product of two or more rotations depends on the order in which they are performed. Comment: Thus, the finite rotation of an object can not be treated as a vector, since the addition of rotations is not commutative.

The rotation of an object is equivalent to the rotation of the coordinate system attached to it, and we shall study the rotation of the body-fixed coordinate system (Figure 6-4).

I. Rotate first through the angle $\phi = 90°$ about the X-axis and then through the angle $\theta = 90°$ about the Z-axis. (Rotations about body-fixed axes.)

II. Rotate first through the angle $\phi = 90°$ about the x-axis and then through the angle $\theta = 90°$ about the z-axis. (Rotations about space-fixed axes.)

$$M_\phi = \begin{bmatrix} 1 & 0 & 0 \\ 0 & \cos\phi & -\sin\phi \\ 0 & \sin\phi & \cos\phi \end{bmatrix} = (\phi = 90°) = \begin{bmatrix} 1 & 0 & 0 \\ 0 & 0 & -1 \\ 0 & 1 & 0 \end{bmatrix}$$

$$M_\theta = \begin{bmatrix} \cos\theta & -\sin\theta & 0 \\ \sin\theta & \cos\theta & 0 \\ 0 & 0 & 1 \end{bmatrix} = (\theta = 90°) = \begin{bmatrix} 0 & -1 & 0 \\ 1 & 0 & 0 \\ 0 & 0 & 1 \end{bmatrix}$$

Applying the rules of matrix multiplication, we obtain (a unit vector in the axis direction is denoted by $\bar{e}$):

I. $M = M_\phi M_\theta$

$$\bar{e}_x \rightarrow \bar{e}_z$$
$$\bar{e}_y \rightarrow -\bar{e}_x$$
$$\bar{e}_z \rightarrow -\bar{e}_y$$

II. $M = M_\theta M_\phi$

$$\bar{e}_x \rightarrow \bar{e}_y$$
$$\bar{e}_y \rightarrow \bar{e}_z$$
$$\bar{e}_z \rightarrow \bar{e}_x$$

In Figure 6-4, I a and II a illustrate the rotations I and II above, and we get the same results as in the matrix calculations. This exemplifies Proposition 1). In the b-versions (in the figure) the order of the rotations is reversed compared to the a-versions, and the different results show that neither rotations about body-fixed axes nor about space-fixed axes are commutative. This exemplifies Proposition 3). The equal results in I a and II b, respectively, and in I b and II a, are two examples of Proposition 2). Here we see clearly how different the interpretations of a certain motion are, depending on whether we prefer the study in terms of rotations about body-fixed axes or rotations about space-fixed axes.

The ambiguity of the rotation angles

There are six different possibilities of describing the rotation about three body-fixed axes, as any of the three axes may be chosen for the first rotation, and after the first choice is made, two axes are left for the second rotation. It seems, however, logical to take the order from X to Y, and this is what we have chosen for our actual calculations. This corresponds to rotating about the space-fixed z-, y- and x-axes, in that order, but by inverting the order for the rotations about the body-fixed axes we can obtain the rotations about the space-fixed axes from x to z.

It is necessary to specify the exact relations of the computational axes to the cardinal directions in the body. A statement such as: "the rotation about the transverse axis is α degrees" is incomplete in describing a composite motion if it is not specified whether the rotation is about a body-fixed or a space-fixed axis, and in which order the rotations are performed. Different orders of rotation yield different values for the rotation angle about the very same axis.

Another possibility in the definition of Eulerian angles deserves to be mentioned. This rotation model does not use three mutually orthogonal rotation axes, but defines the third rotation axis to be equal to the first rotation axis, transformed by the second (intermediary) rotation.

It is in reality this last scheme of rotation angles that is generally understood when Eulerian angles are referred to in the technical literature. Euler's original writing, however, does not specify the rotation model, and any combination of three rotation axes and the corresponding rotation angles that may transform an orthogonal coordinate system into another arbitrarily directed coordinate system should have its angles denoted as Eulerian angles. A comprehensive exposition of the different modes of description is given by Korn and Korn (1968, p. 475).

The product form of the rotation matrix

The transformation matrices M_ϕ, M_ψ and M_θ which represent rotations about the coordinate axes were given earlier in this chapter (Eq. 6:3). The product matrix $M_{\phi\psi\theta}$ for three successive rotations about the body-fixed axes is obtained by direct matrix multiplication of the three matrices,

$$M_{\phi\psi\theta} = M_\phi M_\psi M_\theta = \begin{bmatrix} \cos\psi\cos\theta & -\cos\psi\sin\theta & \sin\psi \\ \sin\phi\sin\psi\cos\theta+\cos\phi\sin\theta & -\sin\phi\sin\psi\sin\theta+\cos\phi\cos\theta & -\sin\phi\cos\psi \\ -\cos\phi\sin\psi\cos\theta+\sin\phi\sin\theta & \cos\phi\sin\psi\sin\theta+\sin\phi\cos\theta & \cos\phi\cos\psi \end{bmatrix}$$

(6 : 6)

The matrix elements are functions of the rotation angles. Having determined the matrix M from experiments, we can obtain the rotation angles by comparing the experimentally determined components with the components given above. This will be discussed in the next chapter.

Small rotations

The mathematical meaning of a "small" (infinitesimal) angle is that the sine and cosine of the angle are approximated by the first term in their series expansion, and that products of angles, being the second order of magnitude, are disregarded. Determining the product matrix for rotations through the small angles $\delta\phi$, $\delta\psi$ and $\delta\theta$, we put $\sin\delta\phi = \delta\phi$, $\cos\delta\phi = 1$, etc., in the separate matrices and perform a matrix multiplication, or we utilize the product matrix just determined and make the insertions there. By either method we obtain:

$$M_\delta = \begin{bmatrix} 1 & -\delta\theta & \delta\psi \\ \delta\theta & 1 & -\delta\phi \\ -\delta\psi & \delta\phi & 1 \end{bmatrix} \qquad (6 : 7)$$

By direct matrix multiplications, it can be shown that this product matrix is independent of the order of the rotations. The product of small rotations is thus commutative, which means that the order of the rotations needs not be specified. Further, if

$$\bar{r} = M_\delta \bar{r}_0$$

Table 16. Errors associated with small-angle approximation. Angles in degrees and values in percent

ϕ	10°	20°	30°
$\sin\phi:\phi$	99.5	98.0	95.5
$\cos\phi$	98.5	94.0	86.6

and we define a vector $\bar{\omega}$:

$$\bar{\omega} = (\delta\phi,\ \delta\psi,\ \delta\theta)$$

we find that

$$\bar{r} = \bar{r}_0 + \bar{\omega} \times \bar{r}_0 \qquad (6 : 8)$$

($\bar{\omega} \times \bar{r}_0$ is the vector product of $\bar{\omega}$ and $\bar{r}_0$; Chapter 8).

To prove that

$$M_\delta \bar{r} = \bar{r}_0 + \bar{\omega} \times \bar{r}_0$$

(small rotations) compute the vector components for each side, using the expressions for M_δ and $\bar{\omega}$ and the rules for matrix and vector products.

The infinitesimal rotation can thus be represented by a vector, the components of which are the rotation angles about the coordinate axes. The composite motion is a rotation about an axis. The direction of the vector $\bar{\omega}$ is the direction of this rotation axis, and the magnitude of the vector is the angle of rotation about the axis. For finite rotations we have exactly the same kind of expression of the motion, i.e. the composite motion is a rotation about one axis. What differs is that we can not break down the finite rotation into rotations about coordinate axes simply by taking the components of a line segment along the rotation axis.

From Table 16 a general impression of the errors associated with small-angle approximation can be obtained. Note, that ϕ in the formula $\sin\phi:\phi$, as well as all angles in this section, except where stated, shall be given in radians.

7. Calculations performed in the computer program "KINEMA"

Introduction. Organization of data

KINEMA stands for kinematics. The purpose of the computer program is to evaluate in terms of rigid-body kinematics, the information gathered in the three-dimensional determinations of positions of indicators in skeletal segments, i.e. information obtained as output from the computer program X-RAY. We have determined the positions of segment indicators for different times, and have this information stored on punched cards. We now want to examine the rigid-body motion, for a certain segment, between the examination times, i.e. determine the "absolute" motion, and in addition to that we want to describe the motion of one segment relative to another. In the task of organizing a set of output information from X-RAY, we collect the different examination times for a certain object, and arrange them in time sequence. The next stage in the subdivision is to arrange the different segments of an object in numerical order, and then we perform a number of operations on these segment-time blocks.

The first operation is a test of the validity of the rigid-body model for each segment. In this test of the rigid-body model we arrange the indicators in a segment in numerical order, and make a closed polygon by linking the indicators. The angles of the polygon and the lengths of its sides are compared, for each time with the first examination time and the preceding one. Further information on the validity of the rigid-body model will be obtained during the determination of the absolute motion.

The part for absolute motion

If there are three or more indicators in a segment of the body common to two times, we can determine the rigid-body motion of the segment between these times. For a particular segment we now, as the next operation, determine the absolute motion between the first time and the successive times (where this determination is possible), and also the motion between subsequent times.

The following kinematic parameters are computed for the motion of a segment:

1) The rotation (Eulerian) angles for rotations about body-fixed X-, Y- and Z-axes in that order.
2) The translation of the centre of gravity of the indicators.
3) An expression for the validity of the rigid-body model.
4) The direction of the rotation (screw) axis.
5) The rotation angle about the screw axis.
6) The translation along the screw axis.
7) The position in space of the screw axis, defined by its intersections with the coordinate planes.
8) The position of the centre of gravity of the indicators.

Computations in Paragraphs 1) and 2) in this scheme give a special presentation of the rotation matrix M and a special translation vector. Paragraphs 4)-7) give the complete determination of screw displacement. The paragraphs of the scheme will now be discussed separately.

The basis for the computations is the determination of the rotation matrix M and the translation vector $\bar{d}$ (Equation 6:1). M and $\bar{d}$ are determined, using a least-squares fitting over all segment indicators common to the two actual examination times. The subroutine of the computer program for carrying out these calculations needs a start approximation.

A start approximation is obtained from solving the equations for three indicators:

$$\bar{r}_{2,\upsilon} = M\bar{r}_{1,\upsilon} + \bar{d} \qquad \upsilon = 1, 2, 3$$

where 1 and 2 stand for the two examination times and υ is the indicator number. However, the matrix thus obtained may not be a rotation matrix.

The components in the calculated matrix are compared with the expression for the product rotation matrix M (Equation 6:6). If the first index in M_{jk} denotes the row, and the second index the column of the matrix, we see that $\sin\psi = M_{13}$. This determines a value of $\psi = \psi_0$, which we choose so that $-\pi/2<\psi_0<\pi/2$. In the next step we obtain from the first row of the matrix:

$$\sin\theta = -\frac{M_{12}}{\cos\psi_0} \qquad \cos\theta = \frac{M_{11}}{\cos\psi_0}$$

which determines $\theta = \theta_0$, and from the third column of the matrix we determine $\phi = \phi_0$,

$$\sin\phi = -\frac{M_{23}}{\cos\psi_0} \qquad \cos\phi = \frac{M_{33}}{\cos\psi_0}$$

As we have both the sine and the cosine of θ and ϕ, the quadrant in which each angle lies is uniquely determined. However, the whole triplet of angles may be substituted in the following way:

$$\phi \rightarrow \phi + \pi$$
$$\psi \rightarrow \pi - \psi$$
$$\theta \rightarrow \theta + \pi$$

This becomes evident by direct insertion of the alternative angles in Equation 6:6 for the matrix. No component is changed by this substitution. The rotation angles are thus not uniquely determined, but this is of no concern to us. When we are interested in the actual values of the rotation angles, they are in the interval ± 90°, so we choose the angle ϕ for which $|\phi|<90°$ (ϕ in degrees). The case $\psi = \pi/2$ is a special case, which we omit from the present discussion.

An alternative method, which we have utilized for a more direct computation of the rotation angles, as it does not utilize the rotation matrix for the determination of the two angles ϕ and ψ, is given by Selvik (1970, p. 37).

After the start approximation ϕ_0, ψ_0, θ_0 and $\bar{d}_0$ is obtained, successive linear least-squares method fittings (subroutine GAUSSA, Wedin 1974) determine the angles of the matrix $M = M_{\phi\psi\theta}$ and the vector $\bar{d}$, which minimize the sum:

$$\sum_{\upsilon=1}^{n}\left(\bar{r}_{2,\upsilon} - M\bar{r}_{1,\upsilon} - \bar{d}\right)^2$$

where n = number of indicators in the segment. The quality of the fitting of the point clusters is expressed by the mean error of rigid-body fitting:

$$ME = e_{rb} = \sqrt{\frac{\sum_{\upsilon=1}^{n}\left(\bar{r}_{2,\upsilon} - M\bar{r}_{1,\upsilon} - \bar{d}\right)^2}{n}} \qquad (7:1)$$

This mean error gives the root mean square distance between a segment indicator moved in a rigid-body motion compared to its actual motion. Of course this includes both deviations from rigid-body behaviour and experimental errors.

The results of this computation are the three Eulerian angles (Paragraph 1), the translation vector $\bar{d}$, which we insert in Formula 6:2:

$$\bar{d}_P = \bar{d} + (M - I)\bar{r}_P$$

to give the translation for P = center of gravity of the indicators (Paragraph 2) and the mean error e_{rb} (Paragraph 3).

Screw displacement: Before we proceed to the computation of the screw displacement, we utilize the matrix M and vector $\bar{d}$ to calculate the positions of the three points (1, 0, 0), (0, 1, 0) and (0, 0, 1) after the motion.

This we do in order to get three points the motion of which is determined from the motion of all of the indicators. We get all the information we have on the rigid-body motion expressed by the motion of these three points.

The direction $\bar{e}$ of the rotation axis (Paragraph 4), and the rotation angle β about this axis (Paragraph 5), can be computed from two vectors between the mentioned points, using a formula of Rodrigues (1840). In modern symbology (Fox, 1967, p. 7) the equations obtained are, if $\bar{a}_0$ and $\bar{b}_0$ are the vectors before and $\bar{a}$, $\bar{b}$ the corresponding vectors after the displacement:

$$\bar{a} - \bar{a}_0 = \tilde{\Omega} \times (\bar{a} + \bar{a}_0) \qquad (7:2)$$
$$\bar{b} - \bar{b}_0 = \tilde{\Omega} \times (\bar{b} + \bar{b}_0)$$
$$\tilde{\Omega} = \tan\frac{\beta}{2}\bar{e}$$

We utilize here the vector product of two vectors (Chapter 8). Screw displacement is illustrated in Figure 7-1.

Note. The direction vector $\bar{e}$ is the eigenvector of the rotation matrix M (Goldstein, 1953, p. 119) and we get a control of the vector $\bar{e}$ determined from Rodrigues' formula in this way. We also can determine the rotation angle β from the matrix M as described by Goldstein (1953, p. 124).

The translation d_S of a point S on the screw axis (Paragraph 6) is equal to the translation of an arbitrary point, P, in the direction of the screw axis, as the total motion of P is a translation along the screw axis and a movement perpendicular to the screw axis. The latter movement is due to the rotation of the body about the screw axis, which moves points in circles, the planes of which are perpendicular to the rotation axis. We thus

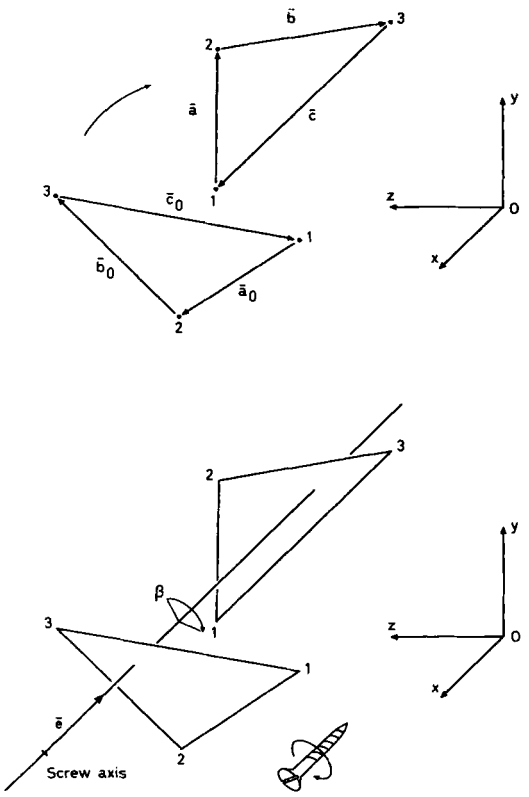

Figure 7-1. A displacement of a rigid body, represented by three points (upper part), described as a screw motion (lower part), with a rotation angle β.

determine d_S, from:

$$d_S = (\bar{r}_P - \bar{r}_{0P}) \cdot \bar{e} \qquad (7:3)$$

utilizing the scalar product of two vectors (Chapter 8). To determine the position $\bar{r}_S$ of a point S on the screw axis, we utilize the definition of the screw axis. The displacement of a point S on the axis is along the screw axis:

$$\bar{r}_S - \bar{r}_{0S} = l\bar{e}$$

where l is a parameter, equal to the translation d_S, as $\bar{e}$ is a unit vector.

By inserting $\bar{r}_{0S}$ from Equation 6:1 we obtain:

$$\bar{r}_S + M^{-1}(\bar{r}_S - \bar{d}) = l\bar{e} \qquad (7:4)$$

A specific point S can be determined from the condition that $\bar{r}_S$ is perpendicular to $\bar{e}$, i.e. $\bar{r}_S \cdot \bar{e} = 0$. The position vector $\bar{r}_S$ is now determined from the last two equations, which also gives the translation $d_S = l$, and the screw axis can be constructed as the line:

$$\bar{r} = \bar{r}_S + t\bar{e} \qquad -\infty < t < +\infty \qquad (7:5)$$

The intersections of this line with the coordinate planes are computed (Paragraph 7). To facilitate the interpretation of the positions of the screw axes we also give the coordinates for the centre of gravity of the indicators in each segment (Paragraph 8).

The part for relative motion

The part of KINEMA for relative motion utilizes information from the part for absolute motion in a very direct manner, as all motion between segments is determined, if the absolute motions of the segments are known.

Relative motion between segments is of interest in two connections. The obvious case is the one in which we want to study a motion between segments, although the absolute motion has full physical meaning. We meet the second case when we, on repetition of an experiment, have an altered orientation between the object and the laboratory coordinate system. We thus get a displacement even for a reference segment, which we want fixed in space. We shall translate and rotate the reference segment back to its first position. We then study the displacement of a second segment from its original position to the position it obtains when this return motion has been performed on the two segments.

The return motion is determined by the reference segment alone, and the relative motion will be given in the laboratory coordinate system, in which the first of the examinations was made.

In both of the cases discussed, we want to study the motion of segment 2 (actual segment) relative to segment 1 (the reference segment) between time 0, reference time and actual time (no index). Of course we could write S_i and S_j for arbitrary segments, and t_k and t_l for arbitrary times, but this extension is obvious and we want to simplify the reading.

If the upper index denotes the segment number, the absolute motion for the two segments in the time interval is:

$$\bar{r}^1 = M^1\bar{r}_0^1 + \bar{d}^1 \qquad (7:6)$$
$$\bar{r}^2 = M^2\bar{r}_0^2 + \bar{d}^2$$

The relative motion $\bar{r}_{2,1}$ (in index 2,1 the first number denotes the actual segment and the second

number denotes the reference segment) is by definition:

$$\bar{r}^{2,1} = M^{2,1}\bar{r}_0^2 + \bar{d}^{2,1} \qquad (7:7)$$

An expression of this form with a relative rotation matrix $M^{2,1}$ and a relative displacement vector $\bar{d}^{2,1}$ is valid, as the combination of two rigid-body motions is a rigid-body motion.

But

$$\bar{r}^{2,1} = (M^1)^{-1}\left(\bar{r}^2 - \bar{d}^1\right) \qquad (7:8)$$

also by definition, as we shall translate and rotate segment 1 back to its original configuration. Note that $M^{-1} = M^T$, the transposed matrix of M, as M is orthogonal (Goldstein, 1953, p. 104).

We can express the relative rotation matrix $M_{2,1}$ and the relative translation vector $\bar{d}^{2,1}$ in terms from the absolute motion. Insertion of $\bar{r}^2$ from Eq. 7:6b in Equation 7:8 gives:

$$\bar{r}^{2,1} = (M^1)^{-1}\left(M^2\bar{r}_0^2 + \bar{d}^2 - \bar{d}^1\right)$$

$$\bar{r}^{2,1} = (M^1)^{-1}M^2\bar{r}_0^2 + (M^1)^{-1}\left(\bar{d}^2 - \bar{d}^1\right)$$

and we find:

$$M^{2,1} = (M^1)^{-1}M^2 \qquad (7:9)$$

$$\bar{d}^{2,1} = (M^1)^{-1}\left(\bar{d}^2 - \bar{d}^1\right)$$

From the relative rotation matrix thus obtained, the rotation angles can directly be determined, using relevant elements of the matrix 6:6. If we want the translation for a certain point, P, of segment 2 relative to segment 1, we go back to the definition formula and find the final relative position $\bar{r}_P$ of P:

$$\bar{r}_0^{2,1} = M^{2,1}\bar{r}_{0P}^2 + \bar{d}^{2,1}$$

The relative translation $\bar{d}_P{}^{2,1}$ of P is

$$\bar{d}_P^{2,1} = \bar{r}_P^{2,1} - \bar{r}_{0P}^2$$

or, utilizing rotation matrices and displacement vectors,

$$\bar{d}_P^{2,1} = (M^{2,1} - I)\bar{r}_{0P}^2 + (M^1)^{-1}\left(\bar{d}^2 - \bar{d}^1\right) \qquad (7:10)$$

We have chosen P to be the center of gravity of the indicators in the actual segment.

For computation of the screw axis motion, we again determine the motion of three idealized points, utilizing now the relative rotation matrix and the relative displacement vector. After this the computations proceed exactly as when determining the absolute motion.

In the part of the program for absolute motion, we computed the rotation matrices and translation vectors for motion from first (reference) time to actual time, and for the stepwise movement between adjacent times. These will be the time combinations in the part for relative motion, but we further restrict ourselves in segment combinations, so we only compute the motion between the first (reference) segment and the actual segment, and between adjacent segments.

It should be noted that when we use some other time than the first as reference time, it is of course the axes in the position at this time about which rotation takes place. When we use the adjacent segment as reference, there is, however, no change in the axes as compared with the first segment as reference, as the directions of the coordinate axes for each segment in the body are the same for one examination.

A test of the method

We have performed tests to control the validity of specific calculations in the computer programme. However, we have not found it feasible to construct an advanced apparatus, functioning as a standard by which we could perform prescribed rotations and translations of a test object, which than could be compared to computed values. This is because the precision of our method is so high, that to make a comparison of standard values with computed values meaningful, would demand much of such an apparatus. We have let it suffice with simple constructions to test the over-all validity of determinations of rotation angles, translations and screw axis position, and have found agreement with the simple "standards". However, the accuracy of our computed values has probably been much higher than the "standard" values. We shall describe a test, utilizing a test cage Model 1B, where the test object is a rigid body (a glass plate) containing 4 marker segments along its longitudinal axis. We displace the body, and examine relative motions between the segments, the "standard" value for which is zero, as the whole body was rigid. The markers (tantalum balls) are five in each segment and form a rectangle, size 60 x 40 mm, with one marker in each corner and one in the midpoint. The distance between the

Table 17. Test of the validity of the computer calculations. Standard errors for rotation (ϕ, ψ and θ) and translation of the center of gravity for a repeatedly evaluated test object with 4 marker segments utilizing test cage Model 1B. Unit:10^{-2} degrees and μm

Motion between	Distance mm	s_ϕ	s_ψ	s_θ	s_x	s_y	s_z
Middle segments	80	3.1	2.9	1.0	10	9	41
Proximal and distal segments	240	3.2	5.3	1.1	29	10	107

Table 18. Test of the validity of the computer calculations. Maximal values for relative motion for rotation (ϕ, ψ and θ) and translation (∂) of the center of gravity for a rigid displaced test object with 4 marker segments utilizing test cage Model 1B. Unit:10^{-2} degrees and μm

Motion between	Distance mm	ϕ	ψ	θ	dx	dy	dz
Middle segments	80	-19	4	-2	69	17	-196
Proximal and distal segments	240	14	-6	-2	157	24	435

segments is 80 mm. The test object lies in the xy-plane of the laboratory coordinate system, with the y-axis forming the long axis of the object. From double evaluations of eight films we found the standard errors for the rotation angles (ϕ, ψ and θ) and the translation (d_x, d_y, d_z) of the center of gravity between 1) the middle segments and 2) the proximal and distal segments (Table 17).

Comment: The precision in determining z-coordinates was in Chapter 5 shown to be 3 times less than the precision in determining x-coordinates, which explains the larger value for the translation error in the z-direction. The "lever arm" is in case 2) above three times the lever arm in case 1), which explains the three times higher values for s_x and s_z in case 2). The fact that s_θ is about one third of s_ϕ or s_ψ is also explained from the lesser precision in the model z-coordinates, which only influences the angles ϕ and ψ.

The mean of the error of the rigid-body fitting (e_{rb}) for the 4 x 8 = 32 evaluations in the test was 24 μm.

We now performed a test in which we rotated the test object into the four positions A, B, C and D, described in Chapter 3. (Figure 3-2). The absolute motions are thus rotations of 180°, but there ought not to be any relative motions between the segments in the test object. With position A as reference position, we obtained the maximal values for any relative motion parameter (Table 18).

The deviations for the angle ϕ and the translations d_x,and d_z might be explained by bending of the film. The errors in angle ϕ and translation d_z are related to each other.

8. Mathematical notations

The position of a point P in space with coordinates x, y and z in a rectangular Cartesian coordinate system with origin O, is denoted by

$$\overline{OP} = \bar{r} = (x,\ y,\ z) \qquad (8:1)$$

We call $\overline{OP} = \bar{r}$ a position vector. To further specify the point P, we can use a lower index and write $\bar{r}_P = (x_P, y_P, z_P)$.

Having two points in space, A and B, with position vectors $\bar{r}_A$ and $\bar{r}_B$, the equation of the straight line passing through the points is

$$\bar{r} = \bar{r}_A + t(\bar{r}_B - \bar{r}_A) \qquad -\infty < t < +\infty \qquad (8:2)$$

Varying t, we obtain the points $\bar{r}$ on the line. The vector $\bar{r}_B - \bar{r}_A$ is the vector from Point A to Point B (Figure 8-1), but can be substituted in Equation 8:2 by any vector along the line joining the points. The equation has three components, and for example the x-component is

$$x = x_A + t(x_B - x_A) \qquad -\infty < t < +\infty$$

Having the vectors, $\bar{a} = (a_x, a_y, a_z)$ and $\bar{b} = (b_x, b_y, b_z)$, where a_x is the component along the x-axis of vector $\bar{a}$, etc., the *scalar product* $\bar{a}\cdot\bar{b}$ of $\bar{a}$ and $\bar{b}$ is

$$\bar{a}\cdot\bar{b} = a_x b_x + a_y b_y + a_z b_z \qquad (8:3)$$

For example, if $\bar{a} = \bar{b} = \bar{r}$, the scalar product

$$\bar{r}\cdot\bar{r} = \bar{r}^2 = x^2 + y^2 + z^2$$

is the squared distance of Point P from origin. The scalar product $\bar{a}\cdot\bar{b}$ of two vectors $\bar{a}$ and $\bar{b}$ can be interpreted as the length of $\bar{a}$ multiplied with the length of the orthogonal projection of $\bar{b}$ on $\bar{a}$.

The *vector product* $\bar{c} = \bar{a} \times \bar{b}$ of the vectors $\bar{a}$ and $\bar{b}$ is defined from its components:

$$c_x = a_y b_z - a_z b_y \qquad (8:4)$$
$$c_y = a_z b_x - a_x b_z$$
$$c_z = a_x b_y - a_y b_x$$

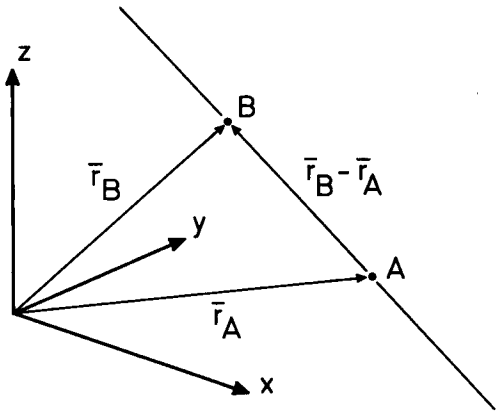

Figure 8-1. The straight line determined by the points A and B with position vectors $\bar{r}_A$ and $\bar{r}_B$.

The components are to be given in a *right-handed coordinate system.* In a right-handed coordinate system, the z-axis points in the direction of the middle finger of the right hand, if the thumb represents the x-axis, and the fore-finger the y-axis. Positive rotations about the coordinate axes are defined by the screw direction of a right-hand screw. This is also the clockwise rotation, when looking in the positive direction of the coordinate axis.

The vector $\bar{c}$ is perpendicular to the vectors $\bar{a}$ and $\bar{b}$ and is directed after a right-hand screw, turned from $\bar{a}$ towards $\bar{b}$. The magnitude of $\bar{c}$ is the length of vector $\bar{a}$ multiplied with the length of the part of $\bar{b}$ that is orthogonal to $\bar{a}$. Note that $\bar{a} \times \bar{b} = -\bar{b} \times \bar{a}$. The names "scalar" and "vector" products are explained by the results, being a scalar and a vector, respectively.

A *matrix M* defines, in our context, an operation on a vector. The matrix has nine components, which we denote M_{ij}, i = 1, 2, 3, j = 1, 2, 3, where the first index denotes the row of the matrix and the second index the column,

$$M = \begin{bmatrix} M_{11} & M_{12} & M_{13} \\ M_{21} & M_{22} & M_{23} \\ M_{31} & M_{32} & M_{33} \end{bmatrix} \qquad (8:5)$$

If the vector $\bar{r} = (x, y, z)$ is the result of the operation of the matrix M on the vector $\bar{r}_0 = (x_0, y_0, z_0)$,

$$\bar{r} = M\bar{r}_0$$

the componants of $\bar{r}$ are

$$x = M_{11}x_0 + M_{12}y_0 + M_{13}z_0 \qquad (8:6)$$
$$x = M_{21}x_0 + M_{22}y_0 + M_{23}z_0$$
$$x = M_{31}x_0 + M_{32}y_0 + M_{33}z_0$$

We can also define the matrix product C of the matrices A and B. If

$$C = AB$$

then the element C_{ik} is given by

$$C_{ik} = \sum_{j=1}^{3} A_{ij}B_{jk} \qquad (8:7)$$

It can be proved that matrix multiplication satisfies the law

$$A(BD) = (AB)D$$

but that in general

$$AB \neq BA$$

The identity or unit matrix I is the matrix

$$I = \begin{bmatrix} 1 & 0 & 0 \\ 0 & 1 & 0 \\ 0 & 0 & 1 \end{bmatrix} \qquad (8:8)$$

From the definition 8:6 it follows that $Ir_0 = r_0$, and from the definition 8:7 it follows that IA = AI = A.

We say that B is the inverse matrix of A if AB = BA = I, and we denote the inverse matrix of A by A^{-1}.

Summary

I have developed a roentgen stereophotogrammetric method for determination of positions of radiopaque markers in an object. The space coordinates are determined in a laboratory coordinate system, which is defined by markers in a test "cage". The markers in the test cage function as calibration points, and are roentgenographed on the same film(s) as the object. Calibration markers and object markers are exposed from two roentgen foci.

The cage markers, are in their function, of two kinds, of which one (fiducial marks) is used for projective transformations of the image points to the laboratory coordinate system, while the other (control points) is used for determining the roentgen foci positions in the same coordinate system. After these calculations have been performed, the three-dimensional coordinates of object indicators are determined by crossing of lines between the roentgen foci and the transformed image points. ,

The mathematical principles for the reconstruction of the bundles of rays from the roentgen foci at the moment of exposure are discussed in Chapter 2. Three constructions of test cages, Models 1A and 1B, and Model 2 are also discussed there. In Test Cage Model 1, the two exposures of the object are obtained on one film, but in Model 2 we expose on two films that are perpendicular to each other. The three cage models are, in turn, intended for high-accuracy determinations of lengths (Model 1A), general determinations of space coordinates, especially in larger objects (Model 1B), and high-accuracy determinations of space coordinates in medium-sized objects (Model 1B). Note, that if the positions of the roentgen foci and the film are not altered, we can roentgenograph the calibration points separately on a film, and then, after removal of the test cage, roentgenograph the object on the same film.

The calibration of the test cages is discussed in Chapter 3. To determine coordinates of markers in a plane is easy, if a rectangular coordinatograph is accessible, and we use the same instrument as for the measurements of the films, a Wild Autograph A8. Determination of the position in space of the plate with control points in relation to the plate with fiducial marks requires more consideration. We describe how the degrees of freedom of the plate with control points (translations in x- and y-directions, rotation angle θ about a z-axis), which are difficult to control at construction of the test cages, can be determined by specific calibration procedures.

Examples of the use of the calibration method are given for test cages of Model 1.

We can now obtain object indicator coordinates, with measured image coordinates and the determined positions in space of the calibration indicators as the input to a computer program which we call X-RAY. In Chapter 4 we discuss the successive steps in the computational procedure, and the information on the quality of the procedure which is printed out. Typical examples of the print-out from X-RAY are given and discussed. Up to March 1974, the computer program has been used for evaluation of more than 1000 roentgenograms.

Chapter 5 deals with the precision in measuring the roentgen films and how errors in the image coordinates of an object influence the model coordinates. We also study the precision in determining the positions of the roentgen foci, and the influence of errors in foci coordinates on the computed model coordinates. A third type of errors studied are those due to remaining errors in the coordinates of the test cage indicators, after the calibration of the test cage. Finally, after having separately studied these origins of errors in model coordinates, we study the total errors in tests, resembling actual utilization of the photogrammetric procedure.

We compare computed values of model coordinates of a test object with "standard" values, thus ascertaining the accuracy of the procedure. We also reevaluate a roentgenogram and compare the two evaluations, thus ascertaining the precision of the procedure.

The standard error s_0 in determining the position of a point on a length-scale was shown to be about 5 μm, when utilizing a test cage of Model 1A, and industrial film.

For a three-dimensional test object, testing area

200 x 90 x 80 mm, and utilizing film in a cassette in combination with a test cage of Model 1B, the mean precision in determining the three-dimensional coordinates of one of the 44 object points was about 50 μm, and the accuracy was about 100 μm (root mean square errors). Utilizing the same test object, and a test cage of Model 2, the precision was found to be about 15 μm without grid and 30 μm with grid (root mean square errors), respectively, and the accuracy was of the magnitude of 30 μm and 50 μm, for the corresponding tests. Calibration errors of the "standard" are included in the values for the accuracy.

A determination of the positions of at least three noncollinear indicators in a rigid body, before and after a movement, makes it possible to study all kinematic aspects of the displacement. In Chapter 6 we discuss possible interpretations of the rotation and translation of a rigid body. The methods are classical, emanating from the work of Leonhard Euler (1776). We further elucidate aspects that are relevant when discussing the kinematics of the skeletal system. The parameters, that ought to be used when discussing the motion of a segment of the skeleton, are determined from the positions of segment indicators utilizing a computer program called KINEMA.

An important aspect of the computations performed is that we are able to study the motion of a segment in relation to another one, even when the two segments have been arbitrarily displaced. An example of the kinematic analysis, utilizing roentgen photogrammetrically determined data, is presented, where we find that the precision, when utilizing a test cage of Model 1B, in determining any rotation angle is of the magnitude of 10^{-2} degrees. The precision in the determination of translations of the center of gravity of a segment in relation to another segment varies with the actual translation direction, but is in principle of the magnitude of tens of micrometers.

Applications

The roentgen stereophotogrammetric method which has been presented in this work is used in studies of the following types:

Studies of the growth of the rabbit tibia. Comparison between the oxytetracycline method and the roentgen stereophotogrammetric method.

Studies of the growth of the long bones (tibia and fibula) to ascertain the effect of treatment with human growth hormone in children with hypopituitarism (In collaboration with S. Aronson and L.-I. Hansson) .

Evaluation of the development of experimentally induced scoliosis in pig. Evaluation of operative treatment of scoliosis in man. Control of the stability of fusions within the spine, with kinematic analysis of the remaining mobility. Both experimental fusions in pig and after fusion operations in man (In collaboration with T. Olsson and S. Willner).

Studies to assess bone healing following maxillofacial surgery by kinematic analysis of the motion during the time of intermaxillary fixation between mobilized and nonmobilized skeletal segments. Studies of positional changes between maxillary segments in infants with cleft lip and palate during growth and after surgery (In collaboration with B. Rune and K.-V. Sarnäs).

Obviously the method can be applied to solve problems in a wide range of areas, and further fruitful applications in both experimental and clinical studies in medicine and dentistry can therefore be anticipated.

Note added in 1989. The three above mentioned areas of research resulted in following three theses:

Aronson A S. X-ray stereophotogrammetry of longitudinal bone growth. Lund 1976.

Olsson T H. A roentgen stereophotogrammetric study of the kinematics of the spine. Lund 1975.

Rune B. Roentgen stereophotogrammetry and metallic implants in the study of craniofacial anomalies. Malmö 1980.

References

Braune W, Fischer 0. Die bei der Untersuchung von Gelenkbewegungen anzuwendende Methode, erläutet am Gelenkmechanismus des Vorderarms beim Menschen. Abh. d. Math.-Phys. Cl. d.k. Sächs. Gesellsch. d. Wissensch. 1885;13:314.

Braune W, Fischer 0. Der Gang des Menschen. Abh. d. Math.-Phys. Cl. d.k. Sächs. Gesellsch. d. Wissensch. 1895;21:152.

Cauchy A-L. Exercises de Mathématiques, II. Paris 1827.

Chasles M. Note sur les propriétés générales du système de deux corp semblables entr'eux. Bulletin Univ des Sciences 1830;14:321

Davidson M. Roentgen rays and localisation. An apparatus for exact measurement and localisation by means of roentgen rays. Brit Med J 1898:10.

Euler L. Formulae generales pro translatione quacunque corporum rigidorum. Novi Comment Petrop 1776;20: 189. Reprinted in Euleri Opera Omnia (2), Basel 1968;9:84.

Fishback W T. Projective and Euclidean geometry. New-York 1962.

Fox E A. Mechanics. New-York 1967.

Goldstein H. Classical mechanics. Cambridge, Mass. 1950.

Greul H. Die medizinische Stereo-Röntgen-Bildmessung in Bereich der Geburtshilfe und Gynäkologie. Düsseldorf 1968.

Hallert B. A new method for the determination of the distortion and the interior orientation of cameras and projectors. Photogrammetria 1954-1955;9:107.

Hallert B. Photogrammetry. New-York 1960.

Hallert B. Determination of the flatness of a surface in comparison with a control plane. The photogrammetric record 1960;3:265.

Hallert B. Elementär felteori för mätningar. Stockhom 1967.

Hallert B. X-ray photogrammetry. Amsterdam 1970.

Hasselwander A. Über die Anwendung der Stereophotogrammetrie des Röntgenbildes in der feldärztlichen Tätigkeit. Münch med Wsch 1915;62:1515.

Hasselwander A. Die objektive Stereoskopie an Röntgenbildern. Stuttgart 1954.

Herron R E. Stereophotogrammetry in biology and medicine. Texas Institute for Rehabilitation and Research. Houston 1972.

Hindmarsh J. Roentgen stereophotogrammetry for evaluating the effect of scolios treatment. Stockholm 1973.

Hjortsjö C-H. Motion and movements. Acta Univ Lund II 1964;4.

Hollender L. Determining the elements of the interior orientation in roentgenography. Acta Radiol 1964; Suppl.230.

Jenkins F, White H. Fundamentals of optics. New-York 1950.

Kendall M, Buckland W. A dictionary of statistical terms. Edinburgh 1957.

Korn G A, Korn T M. Mathematical handbook for scientists and engineers. New-York 1968.

Köhnle H. Röntgenstereoverfahren. Handbuch der medizinischen Radiologie/Encyclopedia of Medical radiology, Berlin 1967;3:220.

Lysell E. Motion in the cervical spine. Acta Orthop Scand 1969;Suppl.123.

Marie T, Ribaut H. Stéréoscopie de précicion appliquée à la Radiographie. C R Acad Sci (Paris) 1897;124:613.

Marie T, Ribaut H. Sur un appareil de mesure simple et général pour la stéréoscopie: le stéreomètre. C R Acad Sci (Paris) 1899;128:1008.

McNeil G. X-ray stereo photogrammetry. Photogram Eng 1966;32:993.

Meier H-K. Der Stereo-Röntgen Komparator StR 1-3. BuL 1971:131.

Nicholls J I, Daly C H, Kydd W L. A stereoscopic X-ray procedure for locating the centroidal axis of the root of a maxillary central incisor. J Biomechanics 1972;5:159.

Patel M. The joint space in normal and osteoarthrotic knees. Stockholm 1973.

Piazzolla-Beloch M. I fundamenti matematici della roentgen-fotogrammetria. L'Universo 1936;17:85.

Rodrigues 0. Des lois géométriques qui régissent les déplacements d'un solide dans l'espace. J Math 1840; 5:380.

Schwidefsky K. Grundriss der Photogrammetrie. Stuttgart 1963.

Selvik G. Den stela kroppens kinematik. Rörelseanatomiska aspekter. Comm Dept Anat Univ Lund 1970;1.

Siegbahn M. La réflexion et la réfraction des rayons X. J Phys Radium 1925;6:228

Singh R S. Radiographic measurements. Photogram Eng 1970;36:1137.

Torlegård K. On the determination of interior orientation of close-up cameras under operational conditions using three-dimensional test objects. Stockholm 1967.

Trendelenburg W. Stereoskopische Raummessung an Röntgenaufnahmen. Berlin 1917.

Wedin P-Å. On the Gauss-Newton method for the nonlinear least-squares problem. The Swedish Institute for Applied Mathematics, Tech Rep 17, Stockholm 1974.

White A. Analysis of the mechanics of the thoracic spine in man. Acta Orthop Scand 1969;Suppl.127.

Appendix: Göran Selvik et coll. Roentgen stereophotogrammetric papers published in scientific journals 1974-88.

1. Aronson A S, Holst L, Selvik G. An instrument for insertion of radiopaque bone markers. Radiology 1974;113:733–4.
2. Rune B, Sarnäs K-V, Selvik G. Analysis of motion of skeletal segments following surgical-orthodontic correction of maxillary retrusion. Application of a new roentgen stereophotogrammetric method. Dentomaxillofac Radiol 1975;4:90–4.
3. Aronson A S, Gustafsson M, Selvik G. Bone growth in the rabbit after irradiation. Acta Radiol (Diagn) 1976;17:838—44.
4. Olin T, Olsson T H, Selvik G, Willner S. Kinematic analysis of experimentally provoked scoliosis in pigs with roentgen stereophotogrammetry. Acta Radiol (Diagn) 1976;17:107–27.
5. Olsson T H, Selvik G, Willner S. Kinematic analysis of posterior spinal fusions in pigs. Acta Radiol (Diagn) 1976;17:369–84.
6. Olsson TH, Selvik G, Willner S. Kinematic analysis of spinal fusions. Invest Radiol 1976;11:1202–9.
7. Olsson T H, Selvik G, Willner S. Kinematic analysis of posterolateral fusion in the lumbosacral spine. Acta Radiol (Diagn) 1976;17:519–30.
8. Olsson T H, Selvik G, Willner S. Vertebral motion in spondylolisthesis. Acta Radiol (Diagn) 1976;17: 861–8.
9. Olsson T H, Selvik G, Willner S. Postoperative kinematics in structural scoliosis. Acta Radiol (Diagn) 1977;18:75–86.
10. Olsson T H, Selvik G, Willner S. Mobility in the lumbosacral spine after fusion studied with the aid of roentgen stereophotogrammetry. Clin Orthop 1977; 129:181–190.
11. Aronson A S, Hansson L-I, Selvik G. Roentgen stereophotogrammetry for determination of bone growth. Comparison with the tetracycline method. Acta Radiol (Diagn) 1977;18:87–93.
12. Rune B, Jacobsson S, Sarnäs K-V, Selvik G. Roentgen stereophotogrammetry applied to the cleft maxilla of infants. I. Implant technique. Scand J Plast Reconstr Surg 1977;11:131–7.
13. Rune B, Jacobsson S, Nilsson M, Sarnäs K-V, Selvik G. Roentgen stereophotogrammetry applied to the cleft maxilla of infants. II. Motion between segments. Scand Plast Reconstr Surg 1977;11:139–46.
14. Aronson A S, Hansson L-I, Selvik G. Roentgen stereophotogrammetry for determination of daily longitudinal bone growth in the rabbit. Acta Radiol (Diagn) 1978;19:97–105.
15. Claesson G, Fredlund P, Mühlow A, Selvik G. Roentgen stereophotogrammetry for evaluation of liver volume and shape. Acta Radiol (Diagn) 1978; 19:423–32.
16. Egund N, Olsson T H, Schmid H, Selvik G. Movements in the sacroiliac joints demonstrated with roentgen stereophotogrammetry. Acta Radiol (Diagn) 1978;19:833–46.
17. Hansson L-I, Olsson T H, Selvik G, Sundén G. A roentgen stereophotogrammetric investigation of innominate osteotomy (Salter). Acta Orthop Scand 1978; 49:68–72.
18. Tropé C, Selvik G, Kullander S, Mattson W, Mühlow A, Åstedt B. Antineoplastic drug effect evaluated with a new X-ray stereophotographic measurement of the tumor volume. Current Chemotherapy 1978:1137–9.
19. van Dijk R, Huiskes R, Selvik G. Roentgen stereophotogrammetric methods for the evaluation of the three dimensional kinematic behaviour and cruciate ligament length patterns of the human knee joint. J Biomechanics 1979;12:727–31.
20. Baldursson H, Egund N, Hansson LI, Selvik G. Instability and wear of total hip prostheses determined with roentgen stereophotogrammetry. Arch Orthop Traumat Surg 1979; 95:257–63.
21. Rune B, Jacobsson S, Sarnäs K-V, Selvik G. A roentgen stereophotogrammetric study of implant stability and movement of segments in the maxilla of infants with cleft lip and palate. Cleft Palate J 1979; 16:267–78.
22. Rune B, Sarnäs K-V, Selvik G. Oral orthopedics and movement of maxillary segments. A roentgen stereophotogrammetric study. Cleft Palate J 1979;16: 385–90.
23. Rune B, Sarnäs K-V, Selvik G. Motion of bone segments after surgical-orthodontic correction of craniofacial deformities. Dentomaxillofac Radiol 1979;8:5–13.
24. Rune B, Selvik G, Kreiborg S, Sarnäs K-V, Kågström E. Motion of bones and volume changes in the neurocranium after craniectomy in Crouzon's disease. J Neurosurg 1979;50:494–8.
25. Baldursson H, Hansson L I, Olsson T H, Selvik G. Migration of the acetabular socket after total hip replacement determined by roentgen stereophotogrammetry. Acta Orthop Scand 1980;51:535–40.

26. Rune B, Sarnäs K-V, Selvik G, Jacobsson S. Movement of the cleft maxilla in infants relative to the frontal bone. A roentgen stereophotogrammetric study with the aid of metallic implants. Cleft Palate J 1980;17:155–74.
27. Rune B, Sarnäs K-V, Selvik G, Jacobsson S. Movement of maxillary segments after expansion and/or secondary bone grafting in cleft lip and palate. A roentgen stereophotogrammetric study with the aid of metallic implants. Am J Orthod 1980;77:643–53.
28. Bylander B, Aronson A S, Egund N, Hansson L-I, Selvik G. Growth disturbance after physial injury of distal femur and proximal tibia studied by roentgen stereophotogrammetry. Arch Orthop Traumat Surg 1981;98:225–35.
29. Bylander B, Selvik G, Hansson L-I, Aronson A S. A roentgen stereophotogrammetric analysis of growth arrest by stapling. J Pediatr Orthop 1981;1:81–90.
30. Rune B, Selvik G, Sarnäs K-V, Jacobsson S. Growth in hemifacial microsomia studied with the aid of roentgen stereophotogrammetry and metallic implants. Cleft Palate J 1981;17:128–46.
31. Tjörnstrand B, Selvik G, Egund N, Lindstrand A. Roentgen stereophotogrammetry in high tibial osteotomy for gonarthrosis. Arch Orthop Traumat Surg 1981;99:73 –81.
32. Rune B, Sarnäs K-V, Selvik G, Jacobsson S. Posteroanterior traction in maxillonasaldysplasia (Binder syndrome). A roentgen stereometric study with the aid of metallic implants. Am J Orthod 1982;81:65–70.
33. Kärrholm J, Hansson L-I, Laurin S, Selvik G. Roentgen stereophotogrammetric study of growth pattern after fracture through tibial shaft, ankle and heel. Case report. Arch Orthop Traumat Surg 1982;99:253–8.
34. Kärrholm J, Hansson L-I, Selvik G. Roentgen stereophotogrammetric analysis of growth pattern after supination-eversion ankle injuries in children. J Pediatr Orthop 1982;2:25–37.
35. Kärrholm J, Hansson L-I, Selvik G. Roentgen stereophotogrammetric analysis of growth pattern after supination-adduction ankle injuries in children. J Pediatr Orthop 1982;2:271–9.
36. Sarnäs K-V, Pancherz H, Rune B, Selvik G. Hemifacial microsomia treated with the Herbst appliance. Report of a case analysed by means of roentgen stereometry and metallic implants. Am J Orthod 1982;82:68–74.
37. Lindahl S, Ranklev E, Selvik G, Ekelund L. Roentgen stereophotogrammetric evaluation of tracheal volumes in the rabbit. Br J Anaesth 1982;54:997–1002.
38. Mogensen B, Ekelund L, Hansson LI, Lidgren L, Selvik G. Surface replacement of the hip in chronic arthritis. A clinical, radiographic and roentgen stereophotogrammetric evaluation. Acta Orthop Scand 1982;53:929–36.
39. Kärrholm J, Hansson L-I, Selvik G. Roentgen stereophotogrammetric analysis of growth pattern after pronation ankle injuries in children. Acta Orthop Scand 1982;53:1001–11.
40. Bylander B, Hansson L-I, Selvik G. Pattern of growth retardation after Blount stapling. A roentgen stereophotogrammetric analysis. J Pediatr Orthop 1983;3: 63–72.
41. Ryd L, Boegård T, Egund N, Lindstrand A, Selvik G, Thorngren K G. Migration of the tibial component in successful unicompartmental knee arthroplasty. A clinical, radiographic and roentgen stereophotogrammetric study. Acta Orthop Scand 1983;54:408–16.
42. Rune B, Sarnäs K-V, Selvik G, Jacobsson S. Roentgen stereometry with aid of metallic implants in hemifacial microsomia. Am J Orthod 1983;84:231–47.
43. Kärrholm J, Hansson L-I, Laurin S, Selvik G. Posttraumatic growth disturbance of the ankle treated by the Langenskiöld procedure. Evaluation by radiology, roentgen stereophotogrammetry, scintimetry and histology: Case report. Acta Orthop Scand 1983;54: 721–9.
44. Alberius P, Selvik G. Roentgen stereophotogrammetric analysis of growth at cranial vault sutures in the rabbit. Acta Anat 1983;117:170–80.
45. Selvik G, Alberius P, Aronson A S. A roentgen stereophotogrammetric system. Construction, calibration and technical accuracy. Acta Radiol (Diagn) 1983;24:343–52.
46. Alberius P, Selvik G. Kinematics of cranial vault growth in rabbits. Am J Anat 1983;168:321–30.
47. Alberius P, Selvik G, Ekelund L. Roentgen stereophotogrammetric analysis of neurocranial suturectomy in rabbits. J Neurosurg 1984;60:158–65.
48. Alberius P, Selvik G. Roentgen stereophotogrammetric analysis of restricted periods of neurocranial suture immobilization in rabbits. J Neurosurg 1984;60: 166–73.
49. Mjöberg B, Hansson L-I, Selvik G. Instability, migration and laxity of total hip prostheses. A roentgen stereophotogrammetric study. Acta Orthop Scand 1984; 55:141–45.
50. Kärrholm J, Hansson L-I, Selvik G. Changes in tibiofibular relationship due to growth disturbance after ankle fractures in children. J Bone Joint Surg 1984; 66-A:1198–210.
51. Kärrholm J, Hansson L-I, Selvik G. Longitudinal growth rate of the distal tibia and fibula in children. Clin Orthop 1984;191:121–8 .
52. Walheim G G, Selvik G. Mobility of the pubic symphysis.In vivo measurements with an electromechanical and a roentgen stereophotogrammetric method. Clin Orthop 1984;191:129–35.
53. Mjöberg B, Hansson L-I, Selvik G. Instability of total hip prostheses at rotational stress. A roentgen stereophotogrammetric study. Acta Orthop Scand 1984;55: 504–6.

54. Alberius P, Selvik G. Volumetric changes in the developing rabbit calvarium. The Anatomical Record 1985; 213:207–14.
55. Huiskes R, Kremers J, de Lange A, Woltring H J, Selvik G, van Rens Th J G. Analytical stereophotogrammetric determination of three-dimensional knee-joint geometry. J Biomechanics 1985;18:559–70.
56. Kärrholm J, Hansson L-I, Selvik G. Mobility of the lateral malleolus. A roentgen stereophotogrammetric analysis. Acta Orthop Scand 1985;56:479–83.
57. Mjöberg B, Brismar J, Hansson L-I, Pettersson H, Selvik G, Önnerfält R. Definition of endoprosthetic loosening. Comparison of arthography, scintigraphy and roentgen stereophotogammetry in prosthetic hips. Acta Orthop Scand 1985; 56:469–73.
58. Rosenquist B, Rune B, Selvik G. Displacement of the mandible during intermaxillary fixation after oblique sliding osteotomy. A stereometric and cephalometric radiographic study. J Max-fac Surg 1985;13:254–62.
59. Ahl T, Dalén N, Holmberg S, Selvik G. Early weight bearing of malleolar fractures. Acta Orthop Scand 1986;57:526–9.
60. Alberius P, Selvik G. Long term analysis of calvarial growth in rabbits. Anat Anz 1986;162:153–70.
61. Alberius P, Selvik G. Postnatal growth of the cranial vault. A review with special reference to the rabbit. Gegenbaurs morph Jahrb 1986;132:519–34
62. Eberhardt K B, Selvik G. Some aspects of knee joint kinematics in rheumatoid arthritis as studied with roentgen stereophotogrammetry. Clinical Rheumatology 1986;5:201–9.
63. Herrlin K, Selvik G, Pettersson H. Space orientation of total hip prosthesis.A method for three-dimensional determination. Acta Radiol (Diagn) 1986;27:619–27.
64. Hägglund G, Bylander B, Hansson L-I, Kärrholm J, Selvik G, Svensson K. Longitudinal growth of the distal fibula in children with slipped capital femoral epiphysis. J Pediatr Orthop 1986;6:274–7.
65. Mjöberg B, Selvik G, Hansson L-I, Rosenquist R, Önnerfält R. Mechanical loosening of total hip prostheses. A radiographic and roentgen stereophotogrammetric study. J Bone Joint Surg 1986;68-B: 770–4.
66. Rosenquist B, Rune B, Selvik G. Displacement of the mandible after removal of the intermaxillary fixation following oblique sliding osteotomy. J Max-fac Surg 1986;14:251–9.
67. Rune B, Sarnäs K V, Selvik G, Jacobsson S. Roentgen stereometry in the study of craniofacial anomalies—the state of the art in Sweden. Br J Orthod 1986;13: 151–7.
68. Ryd L, Lindstrand A, Rosenquist R, Selvik G. Tibial component fixation in knee arthroplasty. Clin Orthop 1986;213:141–9.
69. Selvik G, Alberius P, Fahlman M. Roentgen stereophotogrammetry for analysis of cranial growth. Am J Orthod 1986;89:315–25.
70. Ahl T, Dalén N, Lundberg A, Selvik G. Mobility of the ankle mortise. A roentgen stereophotogrammetric analysis. Acta Orthop Scand 1987;58:401–2.
71. Ahl T, Dalén N, Holmberg S, Selvik G. Early weight bearing of displaced ankle fractures. Acta Orthop Scand 1987;58:535–38.
72. Alberius P, Brant L, Selvik G. Calvarial growth after linear craniectomy in scaphocephaly as evaluated by X-ray stereophotogrammetry. J Cranio-Max-Fac Surg 1987;15:2–9.
73. Mjöberg B, Rydholm A, Selvik G, Önnerfält R. Low- versus high-viscosity bone cement. Fixation of hip prostheses analyzed by roentgen stereophotogrammetry. Acta Orthop Scand 1987;58:106–8.
74. Rosenquist B, Selvik G, Rune B, Petersson A. Stability of the osteotomy site after oblique sliding osteotomy of the manibular rami. A stereophotogrammetric and plain radiographic study. J Cranio-Max-Fac Surg 1987;15:14–9.
75. Rune B, Sarnäs KV, Selvik G. Growth rotation—a puzzle? Europ J Orthodont 1987;9:237–9.
76. Ryd L, Lindstrand A, Rosenquist R, Selvik G. Micromotion of conventionally cemented all-polyethylene tibial components in total knee replacements. A roentgen stereophotogrammetric analysis of migration and inducible displacement. Acta Orthop Trauma Surg 1987; 106: 82–8.
77. Aronson A S, Selvik G. X-ray stereophotogrammetry, a method for high accuracy analysis of growth rate. Acta Paediatr Scand [suppl] 1988; 343:186–7.
78. Ahl T, Dalén N, Selvik G. Mobilization after operation of ankle fractures. Good results of early motion and weight bearing. Acta Orthop Scand 1988;59:302–6.
79. Herrlin K, Pettersson H, Selvik G. Comparision of two- and three-dimensional methods of assessment of orientation of the total hip prosthesis. Acta Radiol (Diagn) 1988; 29:357–61.
80. Herrlin K, Selvik G, Pettersson H, Kesek P, Önnerfält R, Ohlin A. Position orientation and component interaction in dislocation of the total hip prosthesis. Acta Radiol (Diagn) 1988;29:441–4.
81. Herrlin K, Pettersson H, Selvik G, Lidgren L. Femoral anteversion and restricted range of motion in total hip prostheses. Acta Radiol (Diagn) 1988;29:551–3.
82. Herrlin K, Selvik G, Pettersson H, Lidgren L. Range of motion caused by design of the total hip prosthesis. Acta Radiol (Diagn) 1988;29:701–4.
83. Hägglund G, Bylander B, Hansson L-I, Selvik G. Bone growth after fixing femoral epiphyses: Brief report. J Bone Joint Surg 1988; 70-B: 845–6.
84. Kärrholm J, Selvik G, Elmqvist L G, Hansson L-I. Active knee motion after cruciate ligament rupture. Stereoradiography. Acta Orthop Scand 1988;59: 158–64.
85. Kärrholm J, Selvik G, Elmqvist L G, Hansson L-I. Three-dimensional instability of the anterior cruciate deficient knee. J Bone Joint Surg 1988; 70-B:777–83.

86. Lundh H, Westesson P L, Rune B, Selvik G. Changes in mandibular position during treatment with disk-repositioning onlays: A roentgen stereophotogrammetric study. Oral Surg, Oral Med, Oral Pathol 1988; 65:657–62.
87. Mjöberg B, Selvik G. Reduced risk of loosening of hip prostheses with a new cold-curing bone cement. Acta Orthop Scand 1988; 59:343–5.
88. Moell C, Aronson A S, Selvik, G. Growth in rabbits during alternate-day cortisone injections: Near normal growth on days without cortisone. Acta Pædiatr Scand 1988;77:693–8.
89. Rosenquist B, Rune B, Petersson A, Selvik G. Condylar displacement after oblique sliding osteotomy of the mandibular rami. A stereometric and plain radiographic study. J Cranio-Max-Fac Surg 1988; 16:301–7.
90. Ryd L, Albrektsson B E J, Herberts P, Lindstrand A, Selvik G. Micromotion of noncemented Freeman-Samuelson knee prostheses in gonarthrosis. A roentgen stereophotogrammetric analysis of eight successful cases. Clin Orthop 1988;229:205–12.
91. Sarnäs K-V, Rune B, Selvik G, Jacobsson S. Maxillary development in six unilateral cleft lip and palate children treated with passive orthopædic plates. Europ J Orthodont 1988;10:128–36.
92. Wykman A, Selvik G, Goldie I. Subsidence of the femoral component in the noncemented total hip. A roentgen sterophotogrammetric analysis. Acta Orthop Scand 1988;59:635–7.